NANO-MORPHOLOGY OF POLYMER BULK HEROJUNCTIONS STUDIED BY TIME-RESOLVED SYNCHROTRON X-RAY SCATTERING

by

SOO KIM

Presented to the Faculty of the Graduate School of

The University of Texas at Arlington in Partial Fulfillment

of the Requirements

for the Degree of

DOCTOR OF PHILOSOPHY

THE UNIVERSITY OF TEXAS AT ARLINGTON

December 2013

ACKNOWLEDGEMENTS

I am greatly honored to have the opportunity to express my sincere gratitude towards all those people who supported me during my Ph.D. program at the University of Texas at Arlington.

First and foremost, I would like to express the deepest appreciation to my advisor, Prof. Choong-Un Kim and Dr. Michael Jin for leading me into the solar cell industry, offering me the opportunities to get involved into various projects, providing continuous support and assistance throughout my doctoral research. Without their academic guidance and persistent help, I would never have been able to finish this dissertation.

I want to express my special thanks to current and former group members: Dr. Nancy Michael, Dr. Minyoung Kim, Dr. Huili Xu, Rodriguez, Patricia A, Yoonki Sa, Rahmat S Duryat, Pochang, Wendi, Eun-mi Kim, Dr. Jongkwan Lee, Dr. Kihyun Kim, Dr. Eray Erkin, Alex Huang, Yacob, Daniel Wu, Clement, Alex, and Yi Yang for their help and support throughout my research. The moments we shared together, the laughter we had, I will definitely remember them as one of my beautiful times and memories in my life. Without their support and persistent help, this dissertation would not have been possible

I would like to thank to staff members in MSE department: Jennifer Standlee, Libia Cuauhtli, and Beth Robinson for their constant help and encouragement throughout my life at UTA.

I want to thank my parents and wife from the deepest of my heart. Their concern, understanding, encouragement, and devotion have been the essentials to my success. I want to dedicate this thesis to them and express all my gratitude and respects to them. I especially wish to express the most sincere thanks and my love to my wife, Juna Cha who is carrying our baby and is always standing behind me firmly.

Finally, I thank god for allowing me to earn this Ph. D degree.

December 01, 2013

ABSTRACT

NANO-MORPHOLOGY OF POLYMER BULK HETEROJUNCTIONS STUDIED BY TIME-RESOLVED SYNCHROTRON X-RAY SCATTERING

Soo Kim, PhD

The University of Texas at Arlington, 2013

Supervising Professor: Choong-Un Kim

This study investigates the phase transformation of an active layer in organic photovoltaics (OPV) during film deposition and post thermal treatment as well as effects of phase transformation on OPV performance. For this purpose, small - and wide angle X-ray scattering technique (SAXS and WAXS) was applied to examine the phase separation mechanism at relevant fabrication condition of the highest OPV device performance. The poly(3-alkylthiophene)/[6,6]-phenyl-C61 butyric acid methylester (P3AT/PCBM) blend sample was employed in order to study phase transformation of the active layer systemically.

Our exploration with SAXS and WAXS technique found that the polarity of the substrate, a solubility, and solvent evaporation time determine the P3AT/PCBM morphology during the film deposition. On the basis of the results of the peak evolution with time at small and wide angle, the orientation of the P3AT crystal is highly affected by the polarity of the substrate while the type of solvents and their evaporation time can vary the degree of phase separation and P3AT crystallization.

Spinodal decomposition was found to be mechanism for the phase separation of P3AT/PCBM blend driven by PCBM diffusion during post thermal treatment of P3AT/PCBM blend. This finding was obtained from the facts that kinetic of PCBM diffusion is faster than P3AT crystallization and alternating structure with long range order was evolved during the thermal annealing. An image extracted from Force Modulation Microscopy (FMM) further confirms phase separation mechanism of P3AT/PCBM.

Finally, the morphology effects on OPV device performance were elaborated based on the long periodicity and invariant Q value. Since those values can stand for length of phase separation and amount of P3AT crystallization respectively, the importance of the phase separation and P3AT crystallization on the solar cell efficiency was explained. From the direct comparison of long periodicity and invariant Q to OPV device performance, it is found out that both nano-scale phase separation and P3AT crystallization process make contribution on the increment of the solar cell efficiency by enhancing exciton dissociation rate and hole mobility respectively. Moreover, further study using P3OT/PCBM blend showed that degree of phase separation plays a key role to determine OPV device performance more than P3AT crystallization.

TABLE OF CONTENTS

LIST OF ILLUSTRATIONS

Figure Page

LIST OF TABLES

CHAPTER 1

INTRODUCTION

1.1 Research Motivation

Because of the rapid increase of the world's energy demands and environmental issues, fossil fuel is not the one we use as major energy source, but is the target we need to replace it to sustainable energy. Among others, the organic photovoltaic (OPV) has been considered as the most possible alternatives in terms of the low fabrication cost, ease process adaption, and environmental clean device [1.2]. In this reason, extensive studies have been conducted to improve the performance of OPV pursuing more than 10 % of power conversion efficiency (PCE) and less than 1$/Wp cost of module which are the levels that need to be commercialized [3-8].

Despite of continuous efforts made by researchers over the last decades, the PCE of the OPV devices, which is the ratio of output electrical power to input solar power is still not high enough to compete with traditional energy source as well as other type of the photovoltaic devices. One of the main reasons for this low PCE is because of lack of understanding the physics of the organic semiconductor and devices. For instance, the PCE of the OPV device using a mixture between poly(3-hexylthiophene) (P3HT) and Phenyl-C61-butyric acid methyl ester (PCBM) jumped from 0.82 % to 5 % after thermal annealing (140 °C for 15 min) [9]. This dramatic increment is mainly due to the morphological change of P3HT/PCBM thin film driven by nano-scale phase separation and P3HT crystallization process during the post thermal treatment. However, because the fundamental understanding of the morphology formation from

film deposition to post treatment and morphology effects on the device performance are far from the clear, there still remain questions to be answered such that what mechanisms are involved in the phase separation process (nucleation and growth or spinodal decomposition), how to control the active layer morphology, and what morphology condition can makes maximum device performance. Due to these lack of understanding, finding a fabrication condition of the OPV device with the maximum performance become laborious job and can be only achieved by direct comparison of the each experimental condition to its corresponding device performance. To overcome these technical obstacles, it is highly required to elaborate the detail progress of morphology evolution mechanism from the film deposition to post treatment and to study morphology effects on device performance.

Hence, the purpose of this dissertation research is to investigate the morphology evolution of a polymer-fullerene blend and morphology effects on device performance. The primary focus on this study is to identify a phase separation mechanism (binodal or spinodal decomposition) and its driving force (polymer crystallization or PCBM diffusion) in a polymer-fullerene blend system during film deposition and post thermal treatment. Also, the relationship between morphology change and its impact on the device performance is studied. To explore phase separation mechanism and its driving force, Poly(3-alkylthiophene) (P3AT)/PCBM blend has been chosen as a control system since phase separation kinetics can be systemically controlled by P3AT with different side chain length. For this, in-situ Grazing Incidence Small and Wide Angle X-ray Scattering (GISAXS and GIWAXS) technique has been employed during the film deposition and subsequent thermal annealing. The benefits of this technique are able to detect real-time variation of the phase separation and P3AT crystallization during film deposition and post treatment, enabling to study phase separation mechanism and its driving force by extracting the kinetic information of both processes. To study morphology effects on

device performance, the degree of phase separation and P3AT crystallization was calculated in order to compare cell performance directly.

In this chapter, we will briefly review the technology and the physics of OPV device and its technical challenges.

1.2 Organic Photovoltaic Device

1.2.1 Polymer Semiconductors for Organic Photovoltaic Applications

Due to excellent electrical properties and processability, conjugated polymers are considered as the most feasible candidates for the organic photovoltaic applications. Conjugated polymers are made of single and double bonds alternatively. Among others, polythiophene is chosen to explain charge generation and its transportation inside and outside of conjugate polymer [10]. Each carbon atom in the backbone of polythiophene makes σ bonds with only three adjacent atoms, leaving one electron in a p_z orbital as unstable state. This unpaired electron in p_z orbital makes another type of bond (π bond) with nearest electron in p_z orbital along the conjugated backbone. The p_z orbital can divided into π orbital and anti-bonding π* orbital – π orbital is the highest occupied molecular orbital (HOMO) while the anti-bonding π* orbital is lowest occupied molecular orbital (LUMO). This HOMO and LUMO can be considered as valence band maximum and conduction band minimum in inorganic semi-conductor materials. The energy level difference between HOMO and LUMO called band-gap of conjugated polymer, which highly depends on conjugation length [11]. Typically, blue shift of absorption maximum is observed when conjugation length is shorter.

Fig. 1.1 (b) shows the formation of polarons. Theses polarons can be formed by the electron-phonon coupling which is well known in organic materials. In conjugated polymer, polarons formation can be considered as defects in the conjugated polymer chains producing self-trap state. This trap state can hold the electrons since lattice deformations occurs by

phonon effects. These trapped electrons can conduct to another state through hoping process by absorbing or emitting photons to overcome the energy barriers. Hence, in the majority of organic semiconductors, understand of hopping process is so important to understand charge conduction. Fig. 1.1 (c) and (d) shows intramolecular and intermolecular charge transport between back-bone to back-bone and chain to chain [12].

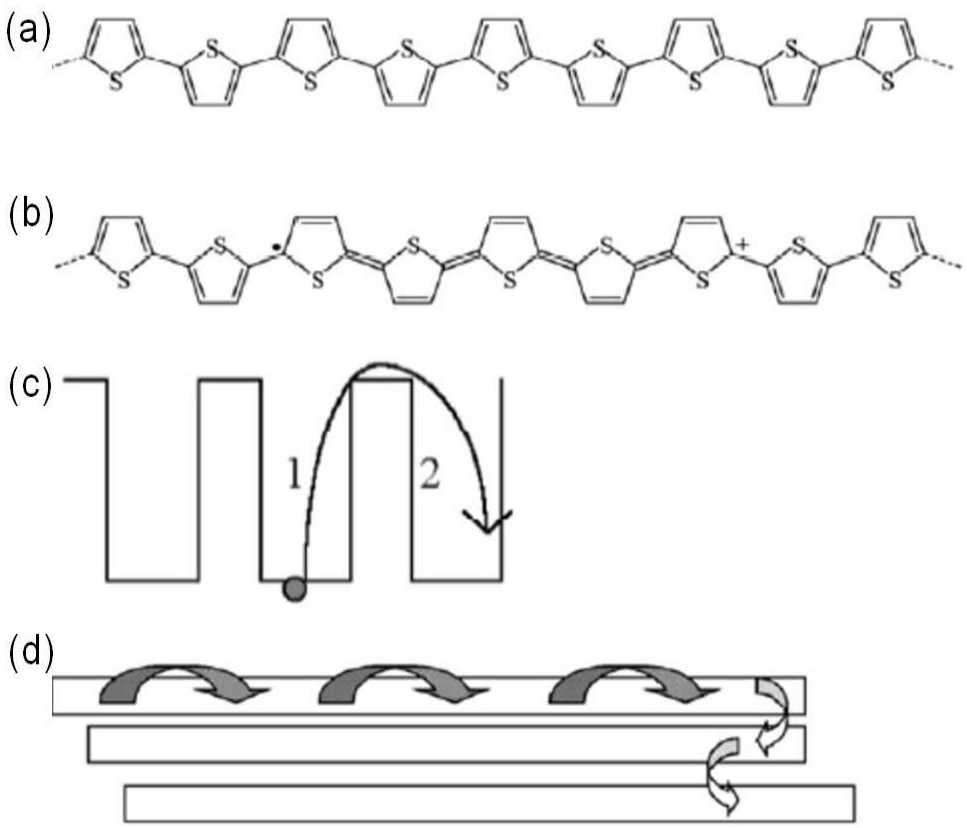

Figure 1.1 Schematic drawing of conjugated polymers and the photophysics: (a), polythiophene; (b), a charged polaron; (c) and (d), hopping process of charge carrier of intra- (filled arrows) and intermolecular (unfilled arrows). [12].

1.2.2 Physics of Organic Photovoltaic Device

The OPV device is a photovoltaic device made of organic polymers or molecules. The primary effect of this OPV device upon the exposure to sunlight is to extract free charge carriers to external circuitry. The Fig. 1.2 shows the basic structure of the OPV device. The active layer, where the photon energy is converted to electrical power is sandwiched between two electrodes and it is made of mixture between donor and acceptor materials.

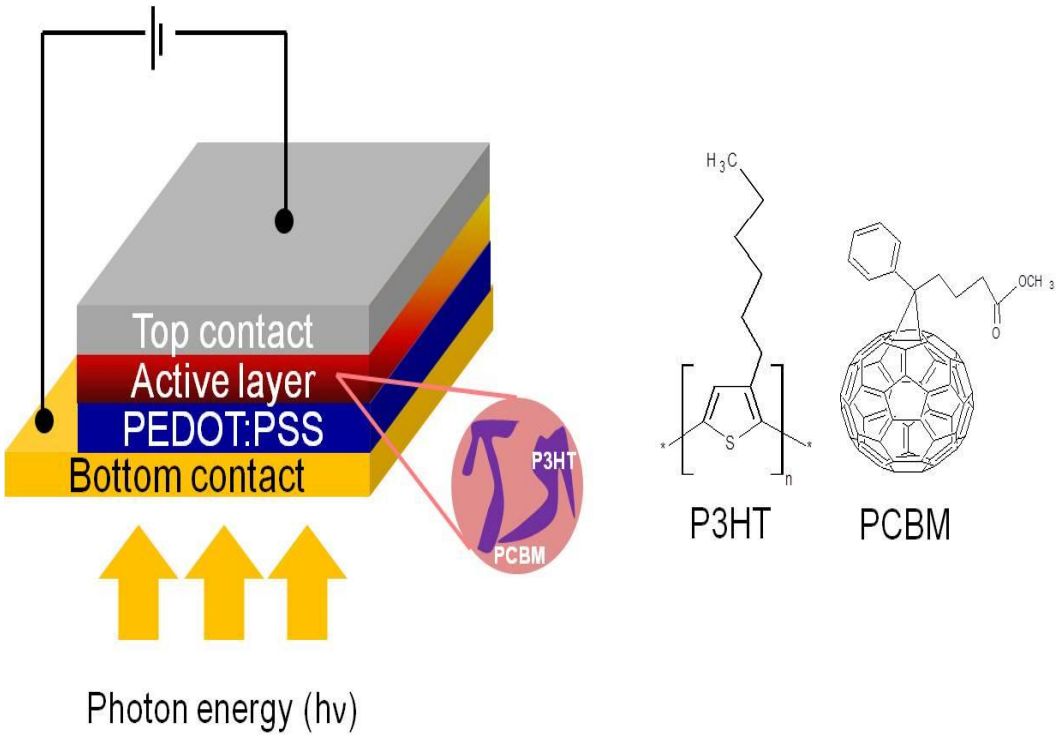

Figure 1.2 Typical structure of an organic photovoltaic based on the P3HT/PCBM blend and chemical structure of P3HT (donor) and PCBM (acceptor) are presented.

Indium-tin-oxide (ITO) coated glass is used as a bottom anode since ITO has high transparency to the sunlight and high work function. Poly(3,4-ethylenedioxyhiophen) : polystyrene sulfonic

acid (PEDOT:PSS) (~ 40 nm) layer is deposited by the spin casting method to reduce the surface roughness and to increase the work function of anode further. The active layer (~100 nm) blended between conjugated polymers and fullerene derivatives is deposited on PEDOT:PSS layer by spin casting method. The Al layer is deposited by using a thermal evaporator as a top cathode due to its low work function and good reflection back to the active layer.

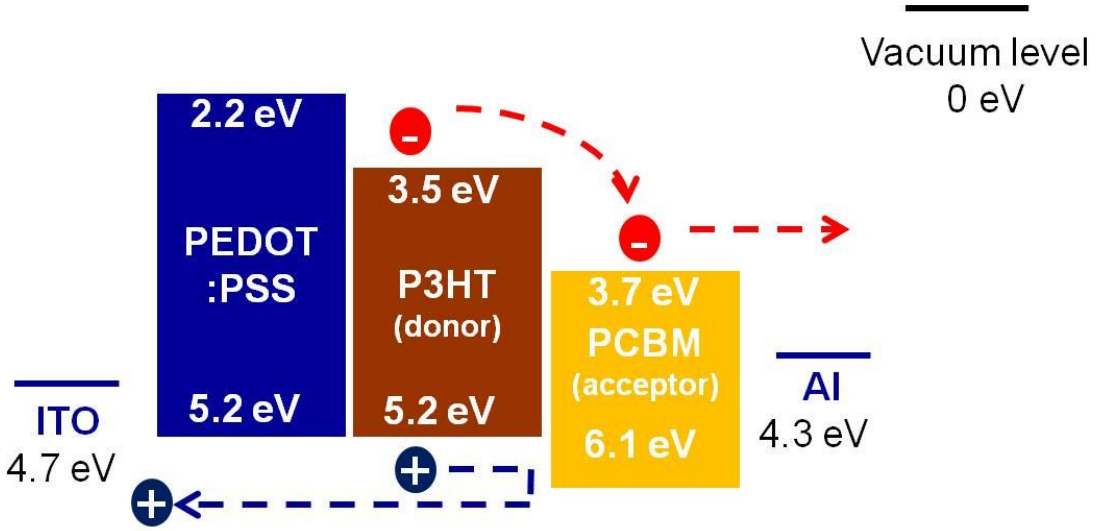

Figure 1.3 Schematic band diagram of P3HT/PCBM organic solar cell.

In organic photovoltaic device, the active layer plays a key role which determines the device performance. Fig. 1.3 explains working mechanism of the OPV device using the typical band structure. When the sunlight reaches to active layer, the excitons (electron-hole pairs) are generated inside of the donor polymer. Those generated excitons are not spontaneously dissociated at room temperature (0.025 eV) since they are strongly bounded by Columbic interactions (0.3 eV) [13]. To make an effective dissociation process, the excitons have to

reach polymer-fullerene interface through the diffusion process since the electrical potential generated by the energy level difference between LUMO levels of the donor and acceptor is higher than the excition binding energy. Right after the separation, the electrons transfer to the acceptor phase while the holes leave in donor phase. The separated electrons and holes moves toward cathode and anode respectively due to the electric field generated by work function difference between top and bottom electrodes. However, all of the excitons do not succeed in charge separation state and reaching to both electrodes. The typical excitons diffusion length is only about 10 nm - 20 nm and the decay process will occur unless they find the polymer-fullerene interface [14]. Furthermore, separated charge carries do not always reach to the both electrodes due to the recombination process such as bimolecular recombination and geminate recombination [15].

1.2.3 Characterization of Organic Photovoltaic Device

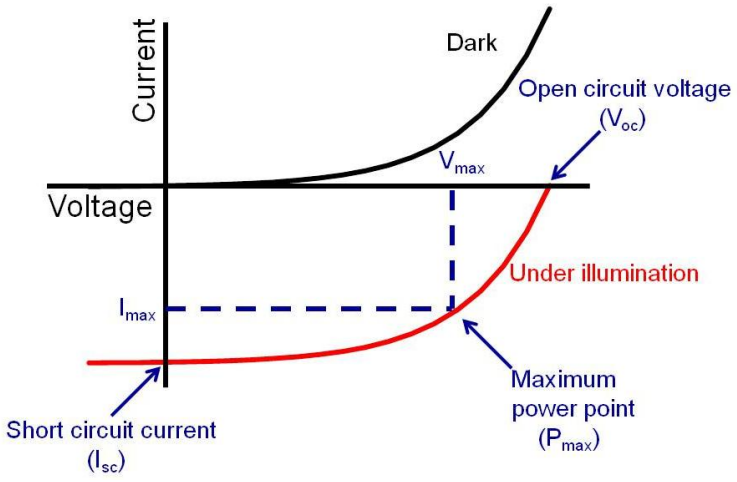

Figure 1.4 I-V curve of an organic photovoltaic device under the dark and illumination condition.

The typical current-voltage (I-V) curve for an organic photovoltaic device is shown in Fig. 1.4. When the device is in the dark (black line), almost no current flow is observed until electrons are injected into the junction larger than a certain value at forward bias region. However, when the cell is under the illumination (red line), the I-V curve are shifted down to the certain value due to the generation of the photocurrent. From the I-V curve, important physical values can be extracted, which can describe the performance of OPV device such as the open circuit voltage (V_{oc}), the short circuit current (I_{sc}), the fill factor (FF), and the power conversion efficiency (η). The open circuit voltage (V_{oc}) is the maximum potential difference between two electrodes under the open circuit states and is directly related to the difference between HOMO level of the donor and LUMO level of the acceptor [13]. The short circuit current (I_{sc}) is the maximum current running through cell without any external voltage. This value is closely related with light absorption of photon by materials and rate of excitions separtion into free charge carriers, the recombination process, and charge collection to the electrodes [16]. The fill factors (FF) is the ratio between maximum power (I_{max} X V_{max}) to product of I_{sc} and V_{oc} while the power conversion efficiency is quotient of maximum power to incident photon energy.

1.2.4 Organic Photovoltaic Device Structure (Bulk Heterojuction)

The organic photovoltaic device has a unique junction structure which is so-called bulk heterojunction (BHJ) while the others based on silicon (Si), copper indium gallium and selenium (CIGS), or cadmium telluride (CdTe) have a bilayer junction structure. The Fig. 1.5 shows the schematic drawing of the BHJ structure made of the mixture between donor and acceptor materials and explains progress of photo-excited excitons separation and charge transportation to both electrodes. From the Fig. 1.5, the major reason for BHJ concept employed to the organic solar cell is to increase the polymer-fullerene interface in order to harvest photo-excited excitons effectively. Photo-excited excitons have to reach the interface where excited

dissociation takes place. However, all of the excitons are not succeed to become free charge carriers due to limited exciton diffusion length (10 nm - 20 nm) [14]. For this reason, the bilayer junction structure cannot be applied to the OPV device since photo-excited excitons generated far below the junction interface will be recombined by exciton decaying process.

So far, BHJ concept has been well accepted to the organic photovoltaic device and developed by introducing various combination of the polymer-fullerene mixture. The Fig. 1-6 shows various combinations of conjugated polymers and fullerene derivatives, employed to organic photovoltaic device so far. The photovoltaic device using the poly(phenylene vinylene) (PPV) mixed with $PC_{61}BM$ showed less than 1 % of PCE in 1995 [17]. Thereafter, the solar cell using P3HT/PCBM had been introduced and its PCE had been evolved up to 4-5 % in 2005. Recently, more than 8 % of the PCE has been reported with mixture between newly synthesized conjugated polymer and fullerene derivatives [18].

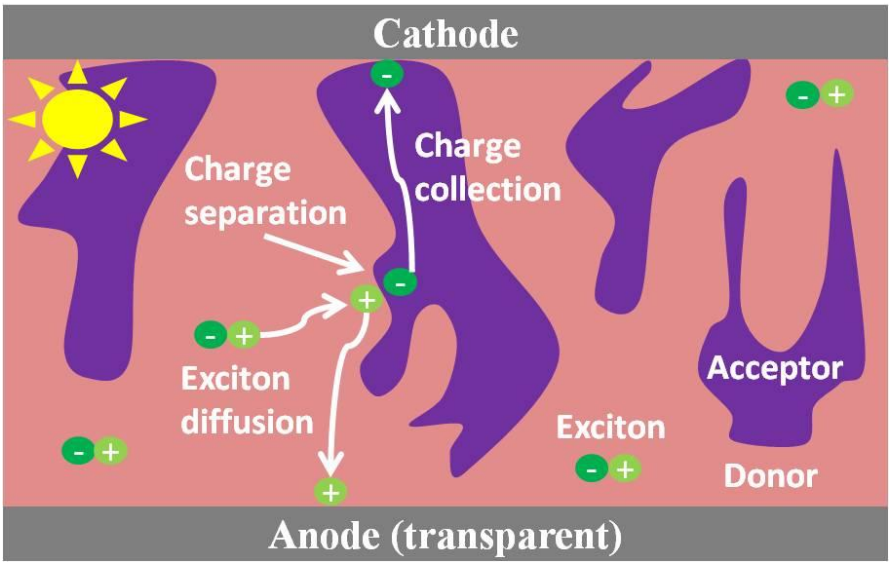

Figure 1.5 Schematic drawing of BHJ structure.

In OPV, one of the factors limiting the device performance was the narrow absorption range in the solar spectrum resulting in significant loss of photons near the low energy side. To overcome this challenge, new conjugated polymers with relatively low band gap has been studied actively to enhance the device performance by capturing more photons.

Moreover, significant efforts have been made on the morphology control to maximize the solar cell efficiency. Since the BHJ structure is based on the blend between conjugated polymer and fullerene derivatives, the excitons dissociation rate and charge carriers transportation are heavily rely on the morphology condition. Optimized morphology of OPV device should satisfy both conditions which are large interfacial area and efficient charge carrier pathway for maximum excitons dissociation and free charge carrier conduction to both electrodes. In this study, morphology evolution by phase transformation of BHJ layer will be mainly discussed.

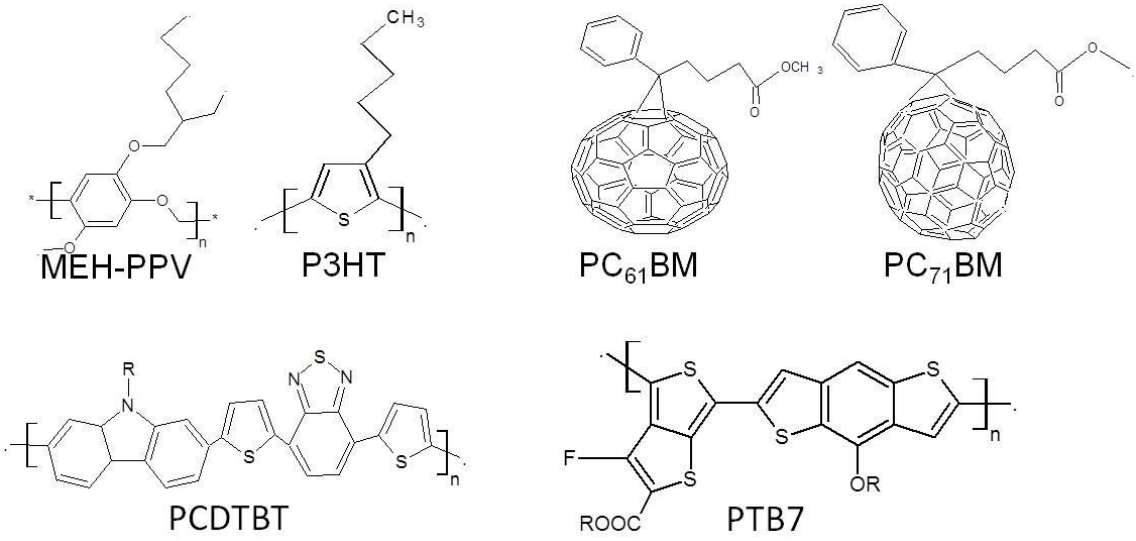

Figure 1.6 Chemical structures of the conjugated polymers and fullerene derivatives

1.2.5 Importance of Morphology

One of the important factors for the best device performance is to realize an optimized morphology between electrons donating and accepting materials. This optimized morphology should satisfy the two conditions simultaneously in order to maximize device performance. The first condition is the formation of nanoscale phase separation between polymer and fullerene. The excitons created from the electrons donor polymers and diffuse to the polymer-fullerene interface in order to be dissociated into electrons and holes. However, if the excitons cannot reach the phase boundaries during the travel, they will eventually recombine by excitons decay process. The second condition is to build efficient carrier pathway since the separated free charges conduct well to the both electrodes to be collected. When the morphology satisfies these two conditions such as nanoscale phase separation as well as efficient carrier pathway, the OPV will show highest photovoltaic performance.

This optimized morphology can be controlled by using the several experimental parameters such as right choice of organic solvent and substrate, composition between polymer and fullerene, solution concentration, and post treatments (thermal and solvent annealing) [19]. In this reason, various approaches have been introduced and attempted to realize the optimized morphology condition [20]. In the case of P3HT/PCBM mixture, PCE remarkably jumped from 0.82 % to almost 5 % after the thermal treatment and this resulted improvement was primarily originated from morphological changes from random mixture to evolution of nanoscale phase separation domain [9].

1.2.6 Morphology Evolution Mechanism

Many researchers around the world have been actively involved in studying a phase transformation on BHJs to understand morphology evolution mechanism. The study using a real time in situ ellipsometry accounted for the role of P3HT crystallization during the phase

separation process [21]. From the result that the onset of the oscillator strength change altered by the P3HT crystallization was faster than the PCBM diffusion, the author demonstrated that the phase separation was mainly induced by the P3HT crystallization. The PCBM diffusion to the nucleation site was followed by the P3HT crystallization process and it occurred through the low polymer density side. Another study using ultraviolet photoemission spectroscopy (UPS) and X-ray photoemission spectroscopy (XPS) provided more detail explanation for the phase separation mechanism in this binary polymer blend [22]. Two step processes was proposed. As a first step, the phase separation between P3HT and PCBM was occurred by spinodal decomposition due to observation of compositional spinodal wave assisted by an interaction between blend component and surface of substrate. The second step was P3HT crystallization process started at the phase boundaries since the interface is energetically and kinetically favorable. Moreover, the competition process between P3HT crystallization and PCBM diffusion as a phase separation mechanism was also suggested by the Chen et al and Wu et al. [23,24]. Although they proposed an analogous phase separation mechanism, the kinetic point of view to determine the phase separation was completely different. Chen et al. insisted that a binodal decomposition driven by the faster PCBM diffusion was the main mechanism for the phase separation. The author explained that the presence of an activation energy during PCBM aggregation is the evidence of the binodal decomposition since the spinodal decomposition does not have a thermo dynamical energy barrier although Wu et al. claimed that the phase separation process was driven by the faster P3HT crystallization by diffusing out the PCBM from the crystal growth front. From the perspective of previous studies, it can be summarized that a driving force and a mechanism for the phase separation is not firmly determined yet and there still remain questions to be answered. Therefore, main goal of this research is to develop

the fundamental understanding of phase separation mechanism from the film formation to the post treatment process.

1.3 Research Objective and Outline of the Thesis

Unlike typical inorganic solar cells those have the bi-layered junction structure, the light-absorbing layer of the polymer solar cell is often casted from a solution of the electron-donating (ED) polymer and the electron-accepting (EA) small organic molecule forming a so-called 'bulk heterojunctions (BHJs)' with a high density of junction interface between ED and EA molecules, which is essential for photo-generated excitons to diffuse and to be dissociated before their recombination.

Several approaches have been applied to produce optimal morphology of what appears to be random in order to enhance the power conversion efficiency of the solar cells - varying solvent evaporation rate, thermal annealing, different concentrations of the molecules, etc. While those efforts have been experimentally successful, the lack of fundamental understanding on the morphological change in BHJ during thermal annealing, for example, blurs the upper limit of the optimal morphology.

Although the spinodal decomposition between the polymer and the small molecule was recently proposed as the main mechanism of the phase separation determining the morphology, kinetics associated with the crystallization of the polymer was not included in the analysis, which could mislead the conclusion.

Hence, the main goal of this research is to develop fundamental understand in phase separation behavior of BHJs and to understand morphology effects on OPV device performance.

The dissertation is organized into six chapters.

In chapter 1, the current technology of OPV device is briefly introduced and the physics of the organic semiconductor and photovoltaic device are reviewed. The current issues of OPV device due to complicated junction structure are discussed. Among them, phase separation mechanism of an active layer in OPV device is emphasized.

In chapter 2, the experimental details will be summarized. The reason for selection of P3AT/PCBM sample will be explained. Then, GISAXS/GIWAXS technique will be overviewed. At last, characterization tools used for analysis of sample evolution will be briefly introduced.

In chapter 3, it is devoted to investigation of phase transformation of P3AT/PCBM during the film deposition using GISAXS/GIWAXS. Effects of a substrate polarity and solvent evaporation time on phase transformation of P3AT/PCBM during thin film deposition are mainly discussed in this chapter.

In chapter 4, phase separation mechanism during thermal annealing will be investigated using SAXS/WAXS technique. The major focus in this chapter is to calculate phase separation kinetic between P3AT crystallization and PCBM diffusion and to understand reasons for peak evolution at small angle side in SAXS/WAXS technique.

In chapter 5, morphology effects on OPV device is discussed. Understanding increment of device efficiency by phase transformation of active layer during thermal annealing and importance between phase separation and P3AT crystallization are major focus.

In chapter 6, the summary of the dissertation and future research will be presented.

CHAPTER 2

MATERIALS AND EXPERIMENTAL TECHNIQUES

2.1 Materials

Poly(3-alkylthiophene) (P3AT) and [6,6]-phenyl C_{61}-butyric acid methyl ester (PCBM) has been used as a control sample to study morphology evolution during the film deposition and subsequent thermal treatment. The combination of the P3AT/PCBM blend makes it possible to study a phase separation mechanism and its driving force systemically since the longer P3AT chain length, the faster PCBM diffusion rate in P3AT/PCBM blend [25].

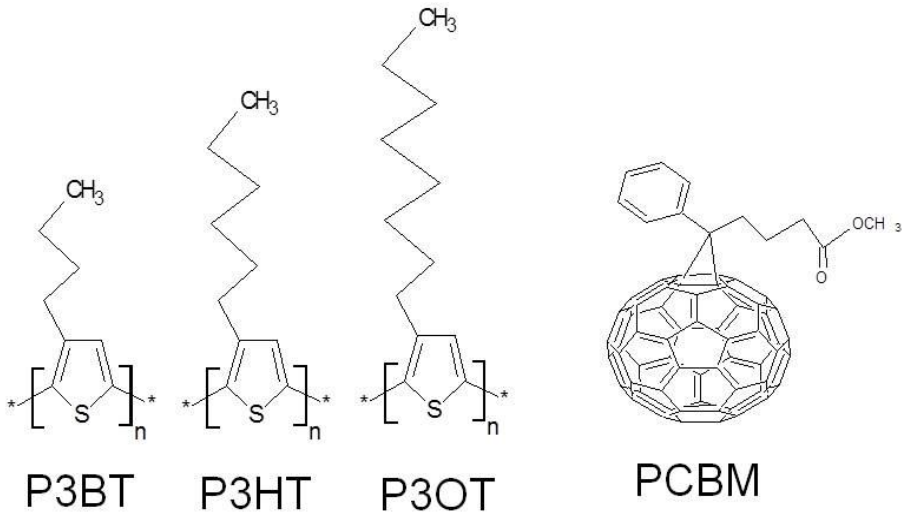

Figure 2.1 Chemical structure of P3AT and PCBM - poly(3-butylthiophene) (P3BT), poly(3-hexylthiophene) (P3HT), and poly(3-octylthiophene)(P3OT).

As described in previous chapter, the phase transformation of P3AT/PCBM blend has been studied during the film deposition and post thermal treatment. To study phase

transformation of P3AT/PCBM during the film deposition, solution-type samples were applied to observe phase separation and P3AT crystallization during solvent evaporation. The sample was prepared by using P3AT (90 mg) and PCBM (90 mg) at 1:1 (wt. %) ratio mixed with chlorobenzene (5 ml). Then, it stirred for 24 hours at 50 °C.

To study the phase transformation of P3AT/PCBM during post thermal treatment, thin film and bulk-type sample was applied. The thin film sample was prepared by using a spin-casting method from P3AT/PCBM solution, while the bulk-type sample was prepared by drop-casting from P3AT/PCBM solution. After solvent dried completely, P3AT/PCBM mixture (20 mg) was taken and it was pressurized to make a rod-shape sample. The bulk-type sample was treated by melt-quenching process in order to remove the thermal history right before measurement.

2.2 Experimental Techniques

2.2.1. X-ray Scattering Technique

2.2.1.1 Introduction

X-ray scattering technique is widely used among the researchers around the world to study crystal structure, chemical composition, and physical properties of materials. This technique can provide information by observing the scattered intensity as a function of scattered angle, polarization, wavelength of scattered X-ray beam. Various scattering techniques have been developed based on types of the scattered beam. Right after interaction between X-ray beam and object, two types of the scattered beam (elastic and inelastic) are produced. Small-Angle X-ray Scattering (SAXS), X-ray reflectivity, and Wide-Angle X-ray Scattering (WAXS) techniques rely on elastic scattered beam. Both SAXS and WAXS technique probes structural evolution and the X-ray reflectivity examines the thickness, roughness, and density of single layer and multilayer thin film. Inelastic X-ray scattered beam is applied to resonant inelastic X-

ray scattering and X-ray Raman scattering techniques. Since this study mainly focuses on phase transformation of P3AT/PCBM blend, SAXS combined with WAXS technique is mainly applied to study morphology evolution of P3AT/PCBM blend. The advantage of this technique is able to to probe the structural change from the angstrom to nanometer size detecting phase separation and P3AT crystallization simultaneously.

2.2.1.2 Principle of X-ray Scattering

The scattering phenomena occurs when an X-ray beam is injected into the matters. Every point in the matter may be regarded as a point which produces secondary waves. Although these secondary scattering waves shows elastic behavior, their diffraction path lengths is not the same, but they differ by their structure or phase distribution.

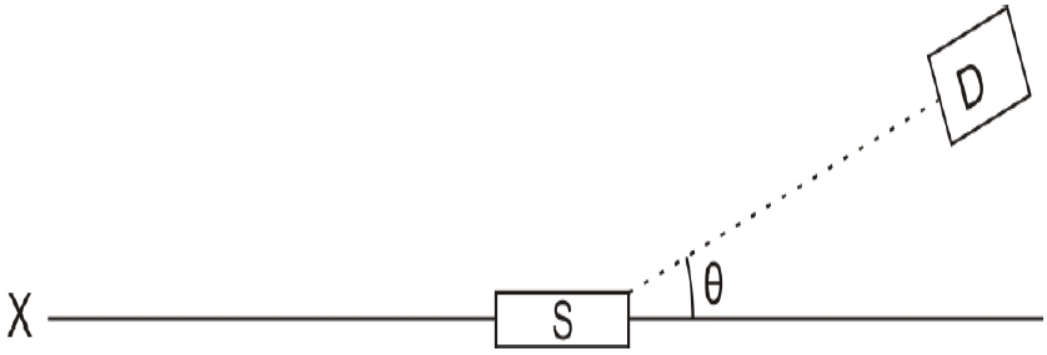

Figure 2.2 Schematic description of an experimental scattering setup [26].

A schematic description of an experimental scattering setup is shown in Fig. 2.2. Monochromatic X-rays beam from the source X is injected into the sample S. Most of the X-ray

beam injected to the sample pass through the sample while only small fraction of the beam make scattering events and detected at an angle θ between incoming X-ray beams and scattered X-ray beams. These scattered X-ray beams are recorded by a detector D depending on the scattering angle θ produced by different phase. An interpretation of the scattering data collected at different scattering angles allows getting structural information of the sample.

The calculation of the phase difference between two points (A and B) at a distance of $\vec{r}$ is shown in Fig 2.3. The scattering vector (q) is defined by [26]:

$$q = \frac{4\pi}{\lambda}\sin\left(\frac{\theta}{2}\right) \tag{2.1}$$

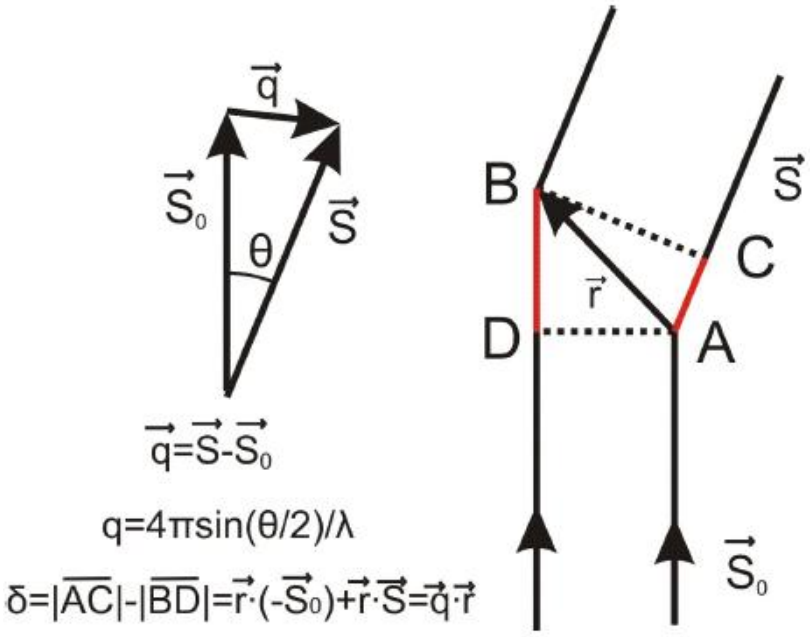

Figure 2.3 Calculation of the phase difference between two scattering points (A and B). $\vec{S}$ and $\vec{S_0}$ is the unit vectors of scattered and incident beam respectively. Θ and $\vec{q}$ stands for the scattering angle and the scattering vector. [26]

where λ is the wavelength of the incident X-ray beam. The scattering amplitude at q is proportional to the electron density distribution ρ(r) in sample and is defined by a Fourier transform. The scattering amplitude at unit volume V is given by [26]

$$A(q) = \int \rho(r) e^{-iqr} dr \tag{2.2}$$

The scattering intensity at unit volume V $I_0\ (\overrightarrow{q})$ can be calculated by complex conjugation of A*(q)

$$I_0\ (\overrightarrow{q}) = A(q) \cdot A^*(q) \tag{2.3}$$

Therefore, total scattering intensity can be concluded by integration of total volume, which incoming X-ray beam is irradiated on sample

$$I(q) = \int 4\pi r^2 dr \cdot \rho(\mathrm{r}) \cdot \frac{\sin(qr)}{qr} \tag{2.4}$$

Due to

$$e^{-iqr} = \frac{\sin(qr)}{qr} \tag{2.5}$$

2.2.1.3 GISAXS and GIWAXS Technique (Thin Film Sample)

GISAXS and GIWAXS technique is part of X-ray scattering technique, designed to study structure evolution. One of the advantages for this technique is able to provide real-time information of the phase separation and the P3AT crystallization simultaneously while the samples are exposed to experimental conditions. The difference between GISAXS and GIWAXS is range of the detection angle, scattered by materials. Typical GISAXS range is up to 0.28 $Å^{-1}$ while GIWAXS is anything above the 0.28 $Å^{-1}$. Fig. 2.4 shows schematic drawing of the experimental GISAXS and GIWAXS setup and patterns of the two scattering rings collected from the P3HT/PCBM thin film sample. To better understand of morphology evolution, time-resolved measurement was conducted during drop-casting of P3AT/PCBM solution and thermal treatment. The incident X-ray beam tilted by 0.12° from the normal direction was injected to

P3HT/PCBM sample. After the incident X-ray beam interacts with sample, two scattering rings were detected at small and wide angle region respectively. These scattering rings were generated by constructive interaction between sample and incoming X-ray beam with certain angle α_f and α_f'.

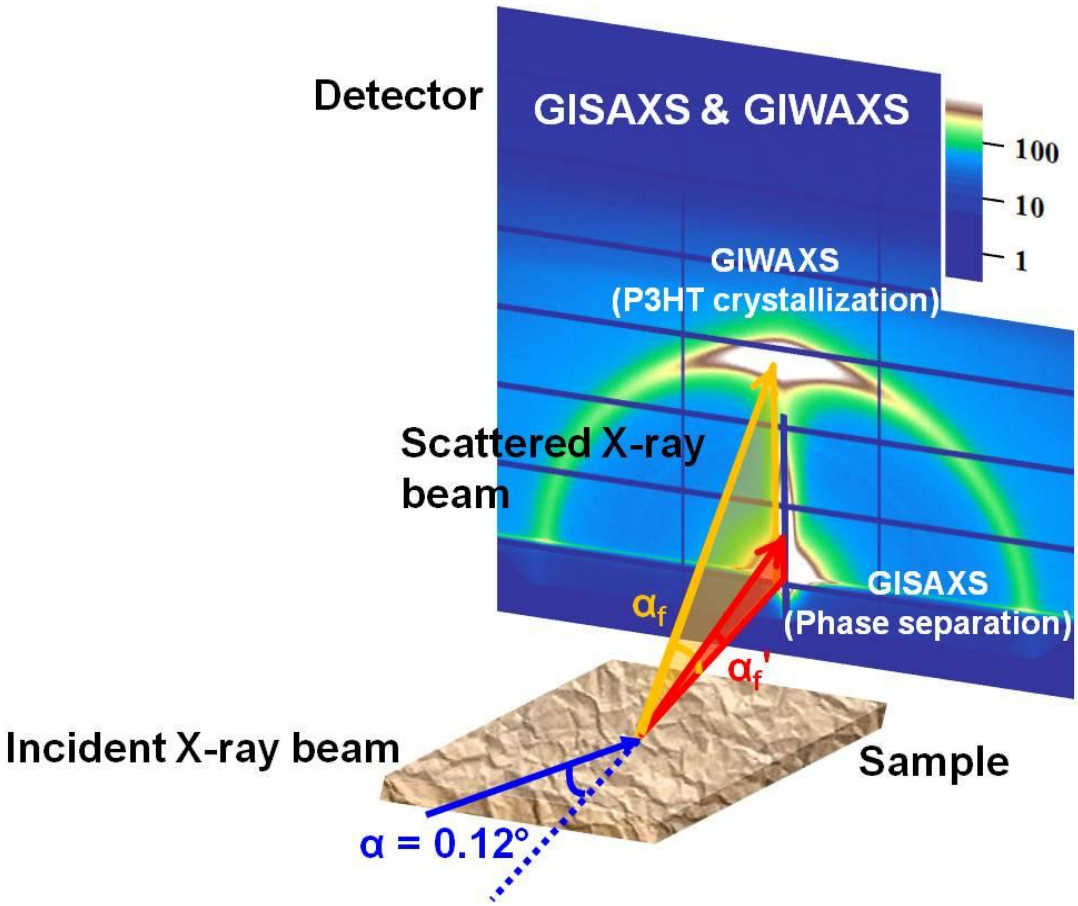

Figure 2.4. Schematic drawing of the experimental GISAXS and GIWAXS setup.

As shown in Fig. 2.3, these scattered rings can be displayed as scattered intensity as a function of scattering vector (q). In GISAXS and GIWAXS, the q is an indicator which describes a distance from the transmitted to the scattered X-ray beam.

In P3HT/PCBM, q at highest scattering intensity were evolved at q = 0.026 $Å^{-1}$ and 0.36 $Å^{-1}$ and their corresponding long periodicity are 23 nm and 2 nm respectively. The previous studies using Transmittance Electron Microscopy (TEM) and X-ray diffraction (XRD) has shown the phase separation length (20 ~ 30 nm) between P3HT and PCBM rich phase and the P3HT d-spacing (2 nm) [27 -29].

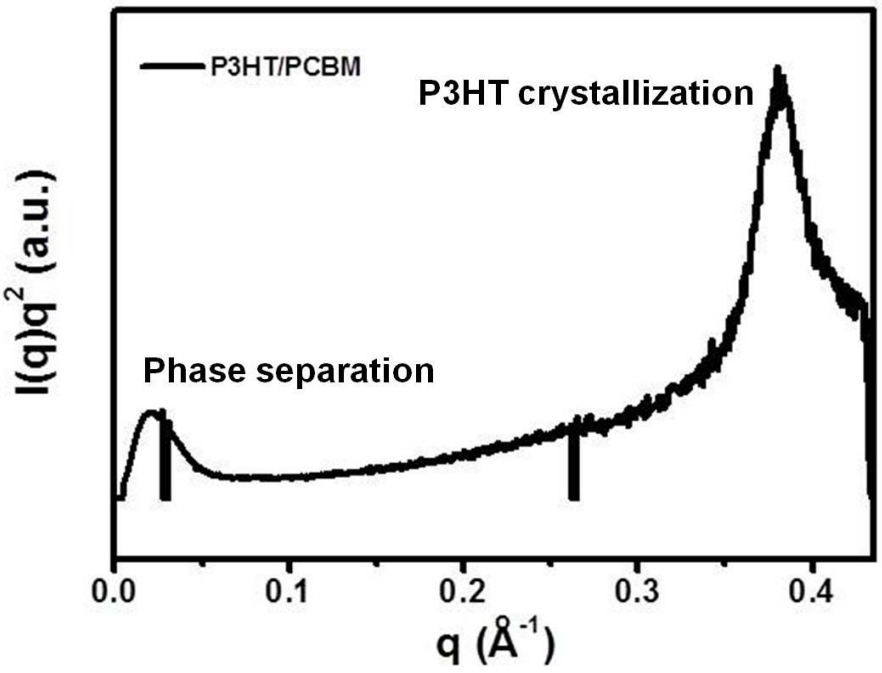

Figure 2.5 GISAXS and GIWAXS scattering data from a P3HT/PCBM.

These reported numbers are quite comparable to the long periodicity calculated from q at GISAXS and GIWAXS, which can represent the signature of the phase separation and P3AT crystallization.

Moreover, the intensity variation at each q can indicate development of the phase separation and the P3HT crystallization since the intensity is directly proportional to a product of two electron density fluctuation, ρ(r) at a distance, r.

$$I(q) = \int 4\pi r^2 dr \cdot \rho(\mathrm{r}) \cdot \frac{\sin(qr)}{qr} \tag{2.5}$$

$$\rho(\mathrm{r}) = < n(r_1) \cdot n(r_2) > \tag{2.6}$$

$$r = r_1 - r_2 \tag{2.7}$$

The $\gamma(r)$ can be calculated by a product of $n(r_1)$ and $n(r_2)$ while $n(r_1)$ and $n(r_2)$ is the difference between electron density at position (r_1) and (r_2) and mean electron density.

2.2.1.4 SAXS and WAXS Technique (Bulk Sample)

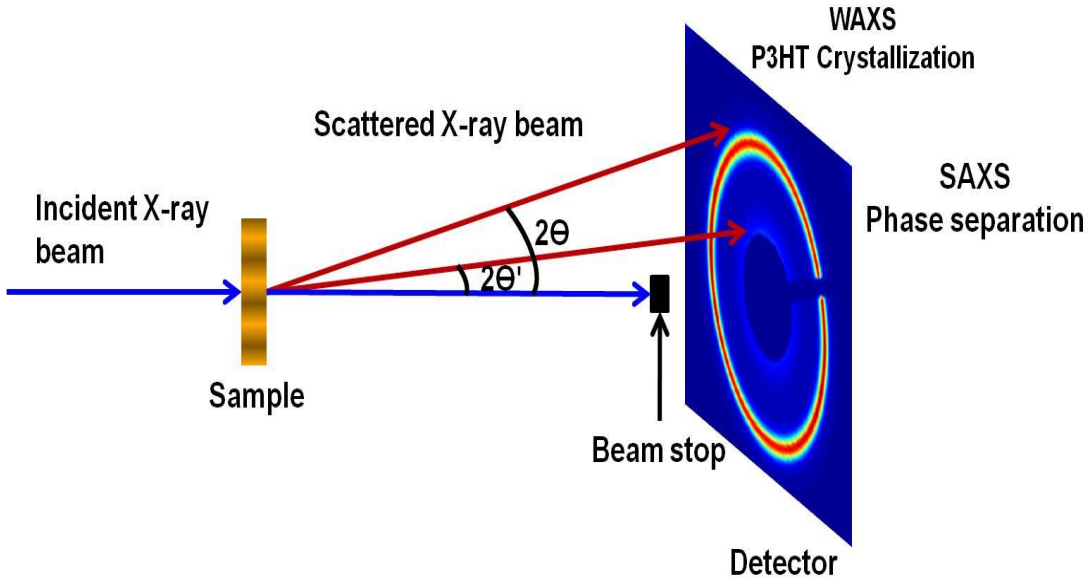

Figure 2.6 Schematic drawing of experimental SAXS and WAXS setup.

SAXS and WAXS technique has been used to detect phase transformation of P3AT/PCBM blend during the post thermal treatment. The Fig. 2.4 shows schematic drawing of SAXS and WAXS experimental setup. The major difference between these two techniques is dimensional character of the scattering. In the GISAXS and GIWAXS, the incident X-ray beam is injected to the sample with critical angles of the P3AT/PCBM film, providing two-dimensional character of the scattering while the SAXS and WAXS can only produce one-dimensional information by introducing X-ray beam perpendicular to the sample. In P3AT/PCBM, signature of the phase separation and P3AT crystallization measured by SAXS and WAXS is comparable to the result of GISAXS and GIWAXS since scattering theory between these two techniques is same. However, in GISAXS and GIWAXS, directional information of P3AT crystal is obtainable additionally due to the incidence angle effect.

2.2.3. Force Modulation Microscopy (FMM)

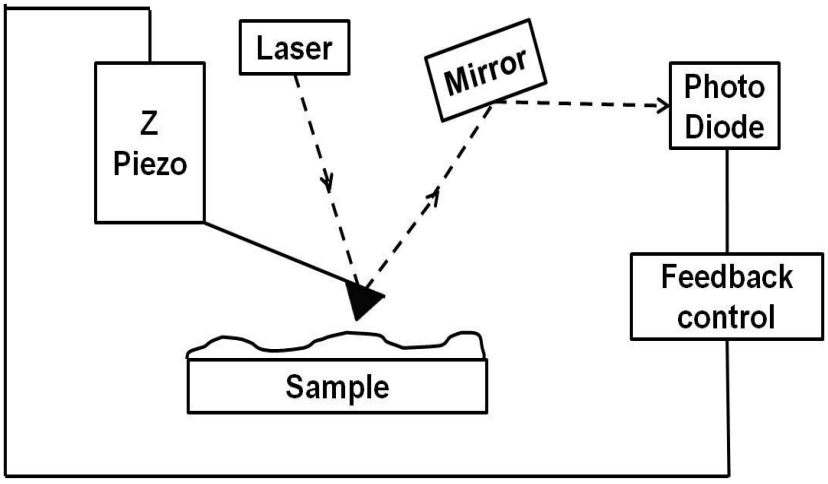

Figure 2.7 Schematic drawing of the force modulation microscopy setup.

The FMM is a part of the AFM technique, operating the under contact mode of AFM. Fig. 2.7 shows schematic drawing of the FMM setup. When a tip scans the sample surface with certain amplitude and pressure, the oscillation amplitude of the cantilever can be varied according to the hardness of the sample surface. During the scan, two types of electrical signal (DC and AC) are generated from the tip and cantilever movement and they produce topography and FMM image respectively. The FMM image is recorded by AC signal which is directly influenced by the elastic properties of the sample surface. The Fig. 2.8 shows a schematic drawing of cantilever deflection at different sample area. Since the soft phase absorbs oscillation, producing smaller amplitude in the AC signal while the hard phase does exactly opposite, the phase difference presented in a sample can be distinguished by the amplitude of cantilever.

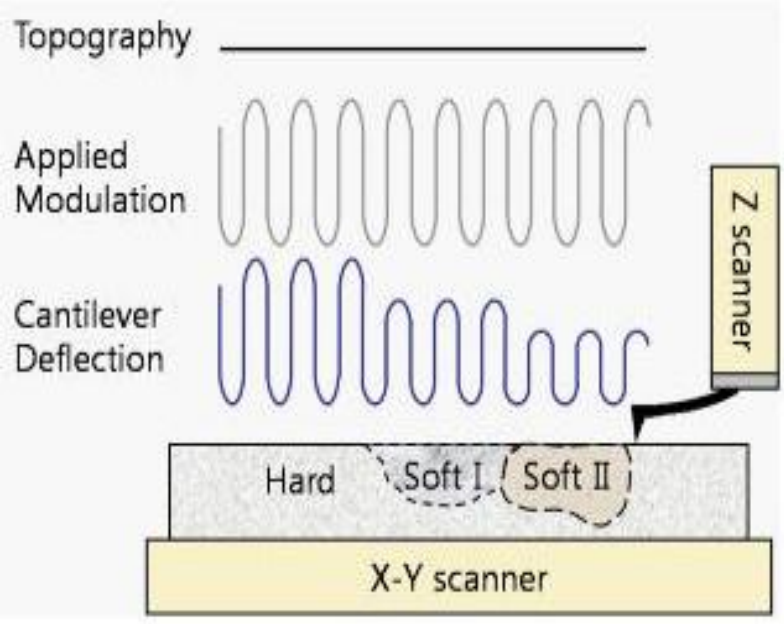

Figure 2.8 Schematic drawing of cantilever deflection at different sample area [30].

As described above, the FMM can be applied to P3AT/PCBM system to observe phase distribution of P3AT rich- and PCBM rich-phase. The Fig. 2.9 is the FMM image of the P3HT/PCBM after spin casting and its unit is nA/Å. From the image, dark and bright areas can be observed and they are assigned as PCBM rich- and P3HT rich-phase respectively since the PCBM is stiffer than the P3HT, producing higher amplitude of cantilever under given current condition [31].

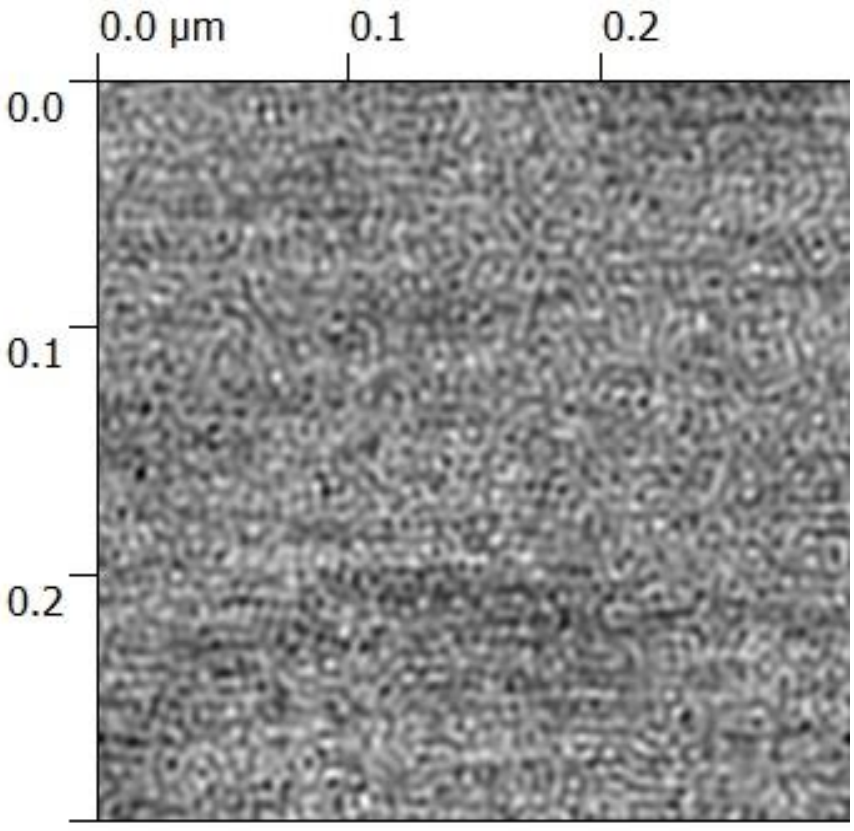

Figure 2.9 FMM image of P3HT/PCBM blend after spin casting.

2.2.4. Current and Voltage (I_V) Characteristic

The current density and voltage (I-V) measurement was conducted under air mass (AM)0 condition. I-V of organic solar cell was measured by home-made solar simulator using a Keithley 2420 3A source meter controlled by computer program written by NASA Glenn Research Center. Projector lamp is calibrated for (AM)0 using the crystalline silicon solar cell calibrated by NASA Glenn Research Center.

CHAPTER 3

THE STUDY OF MORPHOLOGY EVOLUTION IN SOLUTION-CASTED P3HT/PCBM THIN FILM

3.1 Introduction

The bulk heterojunction (BHJ) made of the mixture between electron-donating polymers and electron-accepting small molecules is a typical junction structure employed in organic photovoltaics (OPV). Since the junction interfaces are randomly located through the entire absorption layer and the excitons diffusion length is only about 10 - 20 nm , it is important to accomplish the optimized morphology condition for the efficient charge separation and the subsequent conduction of free charge carriers to electrodes resulting in an efficient power conversion process [32, 33].

In particular, considerable attention has been made to thermodynamics and kinetics of nano-scale phase separation occurring inside BHJ because their fundamental understanding is expected to provide a necessary controllability and reproducibility in fabricating efficient devices [35-37]. In fact, various methods have been applied to drive the necessary phase transformation and phase separation in the BHJ thin-film casted on a substrate and they include thermal annealing, solvent-vapor annealing, and applying an external electrical field after thin film formed by spin casting [38-40].

Prior to the annealing step, the BHJ thin films are mainly formed by a solution-casting of the blend between electron-donating conjugate polymers and electron-accepting fullerene dissolved in an organic solvent. The nature of the solution-casting predicts a significant portion

of the morphological evaluation to occur during the casting stage where the type of the solvents, the solvent evaporation rate, the relative solubility difference, and the interaction between the components and the substrate become important in controlling the morphology [41-44]. The poly(3-hexylthiophene)/[6,6]-phenyl-C61 butyric acid methylester (P3HT/PCBM) solar cell fabricated by spin casting only showed 1.43 % of the power conversion efficiency (PCE) without further annealing step while the post thermal process after the spin casting of this thin film displayed 3% of PCE. This presence of PCE without any post treatment can tell us that BHJ junctions were already formed during the solution-casting process [45].

Some lessons learned from the solvent-vapor annealing can be projected onto the morphological changes that occur during the initial casting process. For example, the PCE of P3HT/PCBM BHJ solar cell was enhanced by 275% by lowering the solvent evaporation rate [46], and, analogously better morphology of the as-casted BHJ thin-film can be possible with a solvent with lower vapor pressure – it is, however, difficult to achieve without changing variables other than vapor pressure at the same time.

Up until now, little is understood about the mechanism of the phase separation during the thin-film casting process prior to the annealing step in BHJ systems. One study showed that the phase separation is mainly induced by the relative difference in the solubility of solutes in a common solvent used for the casting process [44]. The blend solution containing both electron-donating polymers and electron-accepting small molecules can be initially considered as a single-phase homogeneous mixture. Once casted as a thin layer of the solution and the solvent starts to evaporate, phase separation initiates because one solute with lower solubility begins to precipitate from the homogeneous solution layer. As the solvent evaporates further, the film becomes more glassy having two distinctive phases. Moreover, it has been shown that phase separation can also occur by the interaction between the solutes in solution and the substrate.

A study combined with ultraviolet photoemission spectroscopy and X-ray photoemission spectroscopy showed higher P3HT concentration observed on the surface of the film while higher PCBM concentration discovered on the substrate side [47]. This concentration gradient of each solute along the vertical direction was induced by attractive interaction between PCBM and the polar surface of the substrate resulting in the surface directed vertical phase separation.

Kinetics of phase separation in the solid-state film after complete evaporation of the solvent is also still controversial leaving such a question as which process governs the morphological evolution. A study using real time in-situ ellipsometry and by direct comparing the oscillator strength changes for P3HT and PCBM showed that the P3HT crystallization process occurred faster than the PCBM aggregation process and the PCBM diffusion process to the nucleation site started after the onset of P3HT crystallization [48]. However, another kinetic study using grazing incidence small-angle X-ray scattering (GISAXS) and grazing incidence wide-angle X-ray scattering (GIWAXS) and analyzing data with Avrami-Johnson-Mehl (AJM)

To achieve high efficient polymer solar cell, well understanding of the phase separation mechanism and its kinetics during the solution-casting is highly desirable to control the thin film morphology. Here, we demonstrate the morphology evolution of the P3HT/PCBM BHJ thin film by using the time-resolved GISAXS and GIWAXS technique. The P3HT/PCBM thin film samples prepared by different solvent evaporation rate (spin-casting and solution-casting) were applied to observe how the phase separation and P3HT crystallization proceed during the morphology evolution and to study the correlation between morphology evolution and solubility and substrate effect. Moreover, from the comparison of progress of phase separation and P3HT crystallization obtained by GISAXS and GIWAXS simultaneously, mechanism of phase

separation will be discussed combined with kinetics of phase separation and P3HT crystallization.

3.2 Experiments

3.2.1 Materials

Regioregular poly(3-hexylthiophene) (P3HT) and [6,6]-phenyl C_{61}-butyric acid methyl ester (PCBM) were purchased from Sigma Aldrich. The regioregularity of the P3HT is 91 ~94 % and the molecular weight is Mw 50 ~ 70 K.

3.2.2 P3HT/PCBM BHJs Thin Films Fabrication

The P3HT/PCBM blend solution (1:1 ratio) in chlorobenzene (36mg/ml) was stirred for one day under a fume hood. The solution-casting and spin-coating process (1000 rpm for 1 min) was conducted on silicon substrates under the ambient condition to fabricate the BHJ thin films.

3.2.3 GISAXS/GIWAXS

The X-ray beam line (12-1D-B) at advanced photon source in argonne national laboratory was used for the scattering experiments. The sample to detector distance was the 1695.3 mm and PILATUS 2M detctor was used for the measurement. the X-ray energy was the 12 KeV and the incident angle was the 0.12°. The GISAXS and GIWAXS measurement was started right after the casting of P3HT/PCBM blend solution on the silicon substrate and it continued until the sample become solid state film.

3.3 Result and Discussion

X-ray scattering has been widely used to study the phase separation in polymer blends [50,51]. Fig. 3.1 presents the schematic of experimental setup for GISAXS and GIWAXS techniques used in this study. The incident X-ray beam entered into a thin-film sample at 0.12° off the substrate plane and the coherently scattered beam from the sample was recorded using a two dimensional detector. The two ring patterns recorded on the detector (Fig. 3.1) are assigned to

(100) planes of P3HT crystals (outer circle) and the phase separation between P3HT- and PCBM-rich domains (inner circle) respectively [52]. The outer circle provides the directional information of the P3HT crystals. As depicted in Fig. 3.1, if the π-π stacking direction is parallel to the substrate, the direction of P3HT crystals are assigned to edge on direction while P3HT crystals to the face on direction show the π-π stacking direction is perpendicular to the substrate. Accordingly, the advantages of the GISAXS and GIWAXS technique is to provide the progression of P3HT crystallization and the phase separation in the P3HT/PCBM BHJ thin film on a real time basis, which can explain the morphology evolution of P3HT/PCBM thin film.

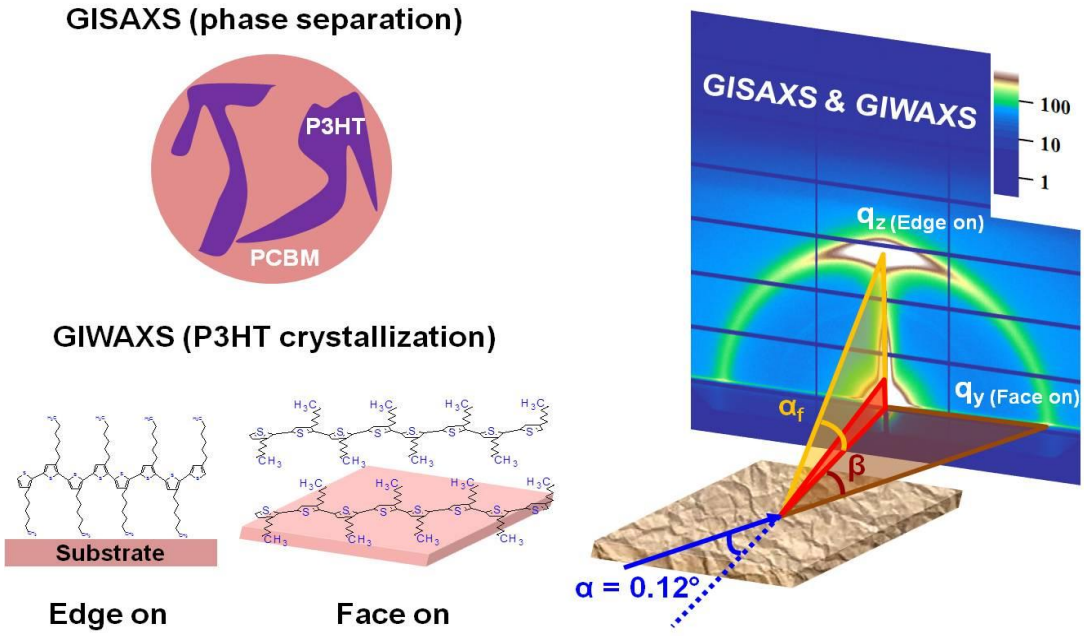

Figure 3.1 Schematic drawing of GISAXS and GIWAXS experimental setup. α is the incident grazing angle to the sample while α_f and β are the scattering angle for the edge-on and face-on planes of P3HT crystals respectively. The outer and inner ring patterns recorded on a two-dimensional detector are assigned to (100) planes of P3HT crystals and phase separation between P3HT-rich and PCBM-rich domains respectively.

Fig. 3.2 displays a series of X-ray scattering images of a P3HT/PCBM BHJ film recorded for about 10 mins right after its spin casting process. The spin casting was conducted on a silicon substrate for 1 min at 1000 rpm at room temperature. The line-cut method was employed to obtain scattering intensity at each azimuthal angle of the P3HT crystals.

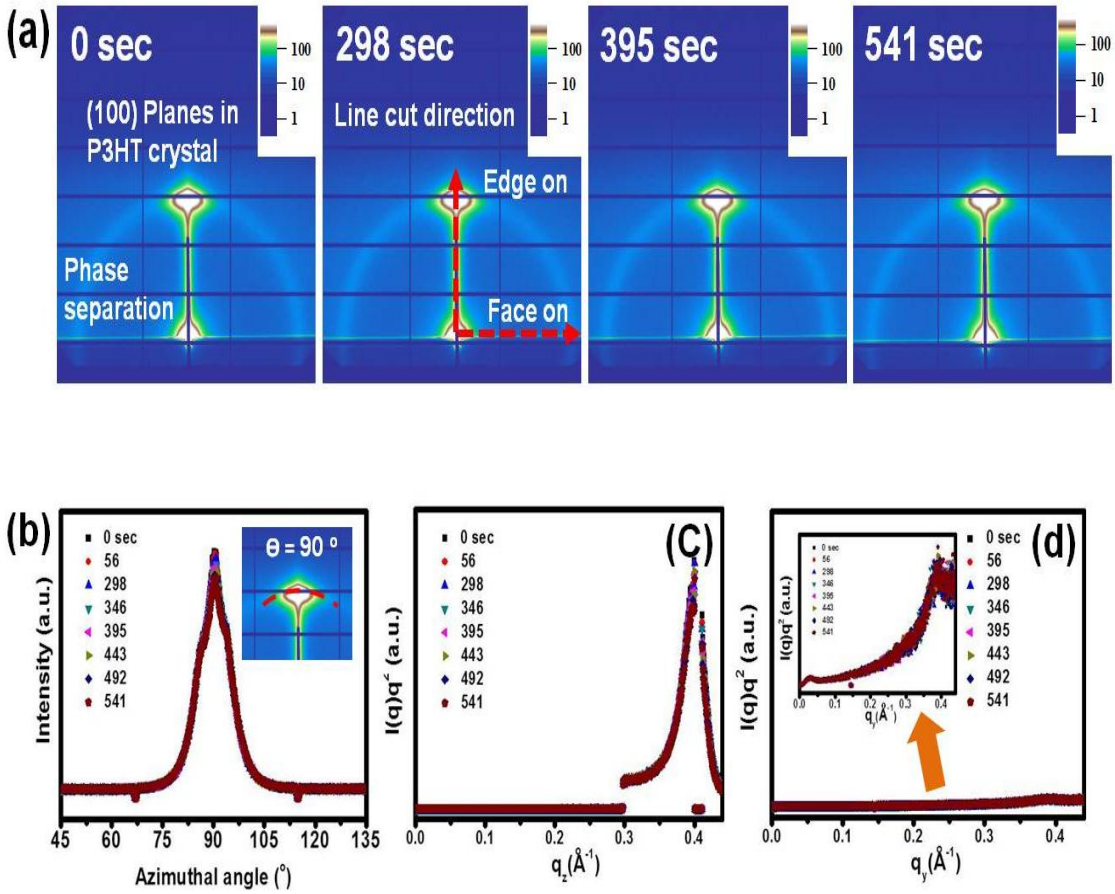

Figure 3.2 Time-resolved GISAXS and GIWAXS images (a), the corresponding intensity variation of azimuthal angle (b), and the Lorentz-corrected X-ray scattering peaks to both edge direction (c) and face on direction (d) are displayed for spin-casted P3HT/PCBM thin film. The onset figure in Fig. 3.2(d) is the 27 times enlargement of X-ray scattering peak to the face on direction.

In Figs. 3.2 (b), (c) and (d), azimuthal angle distribution for P3HT crystals and Lorentz-corrected X-ray scattering peaks oriented to the edge and the face on direction was presented as a function of time. From onset figure in Figs. (d), two scattering peaks were shown at scattering vectors of 0.02 $Å^{-1}$ and 0.39 $Å^{-1}$ which assigned for phase separation and (100) planes of P3HT crystals respectively [53,54].

The angular spread of the P3HT crystals obtained by FWHM of (100) planes of P3HT crystals peak is around 10°. Higher peak intensity for (100) planes of P3HT crystals oriented to the edge on direction was observed while lower intensity for phase separation and (100) planes of P3HT aligned to the face on direction was detected. The phase separation peak at edge on direction was not shown because the some part of line-cut pathway was superimposed on the beam stop area. The interesting features in Fig. 3.2 are that the angular spread of P3HT crystals and X-ray scattering peaks were not varied as a function of time even though the measurement was conducted right after the spin casting and the (100) planes of the P3HT crystals is mainly aligned to the edge on direction only. These non-diversity of X-ray scattering peaks at both phase separation and P3HT crystallization and formation of P3HT crystals with preferential orientation can explain that the formation of P3HT/PCBM morphology by P3HT crystallization and PCBM diffusion process is already complete during the short period of spin casting process and the force which makes P3HT crystals having favored orientation is generated.

In a ternary system, the phase separation and the crystal growth with preferential orientation can be determined by mutual interaction of solutes components with a substrate and an organic solvent. Similarly, the P3HT/PCBM morphology prepared by spin action was induced by those interaction which is relative solubility difference against the solvent and substrate effect. This interaction is so important to understand how these components interplay

each other during the morphology evolution and how fast the morphology evolve by these components since the morphology is directly correlated with solar cell performance.

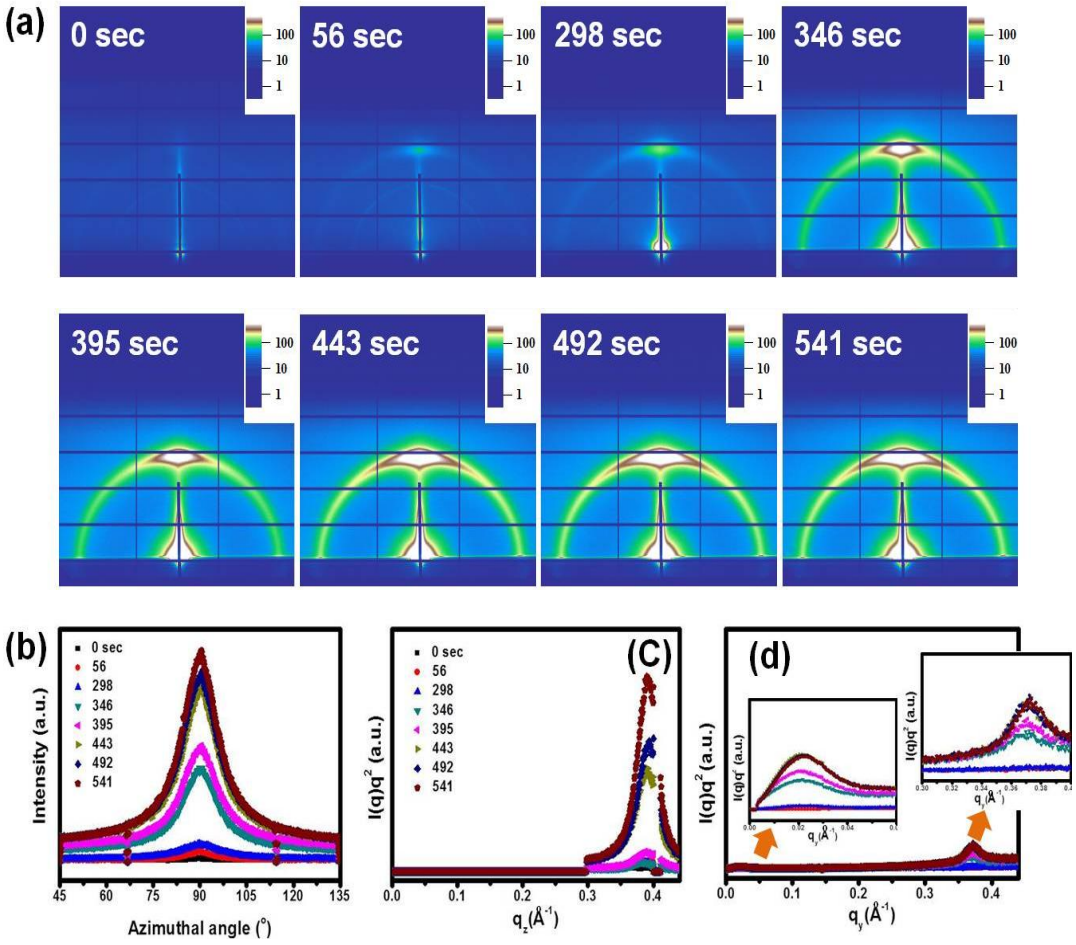

Figure 3.3 Time-resolved GISAXS and GIWAXS images (a), the corresponding intensity variation of azimuthal angle (b), and Lorentz corrected X-ray scattering peaks for both edge on direction (c), and face on direction (d) are displayed for the solution-casted sample The onset figures in Fig. 3.3(d) is the enlargement of X-ray scattering peak to the face on direction. The left one is 50 times enlargement of phase separation peaks between the scattering vector q = 0 $Å^{-1}$ and 0.06 $Å^{-1}$. The right one is 5 time enlargement of (100) planes of P3HT crystals between scattering vector q = 0.3 $Å^{-1}$ and 0.4 $Å^{-1}$.

To study this morphology evolution by solubility difference and substrate effect, we designed the experimental condition which applies slow solvent evaporation rate compared to the spin-casting to closely examine how those factors act on phase separation and P3HT crystal orientation during the solicitation process, and the evolution in the blend morphology was recorded by employing time-resolved GISAXS and GIWAXS techniques.

Fig. 3.3 displays a series of X-ray scattering images obtained for about 10 mins after a thin layer of blend solution was casted on the silicon substrate without spinning the sample. The sample was kept under ambient conditions during the measurement. Azimuthal angle-dependent scattering intensity from (100) planes of P3HT crystals was extracted by applying the line-cut method and the obtained X-ray scattering data was Lorentz-corrected. Unlike the X-ray scattering images from the spin-casted sample, the data from the solution-casted sample shows the sample has experienced several stages of the phase transformation. At the beginning (0 sec), all the solvent and solute molecules in the film are homogeneously mixed together and none of crystal growth and phase separation was observed. At 56 sec, (100) planes of P3HT crystals aligned at the edge-on direction started to appear while neither the phase separation or (100) planes of P3HT crystals at the face-on direction was observed. This state continued until 298 sec. After 298 sec, the phase separation was shown firstly and the direction of the P3HT crystals started to vary from the edge on to the face on direction. As times went further, the phase separation and P3HT crystals to the both directions grew rapidly and they has reached its stable state at about 492 sec while P3HT crystals to the edge on direction continued to grow until 590 sec. After the 590 sec, overall phase transformation has approached to the stable state, confirmed with Fig. 3.4.

From observation in Fig. 3.3, the morphology evolution in P3HT/PCBM blend can be

divided by three steps. The first step is the emerging of P3TH crystals oriented to the edge on direction only while none phase separation and P3HT crystals aligned to the face on direction was observed.

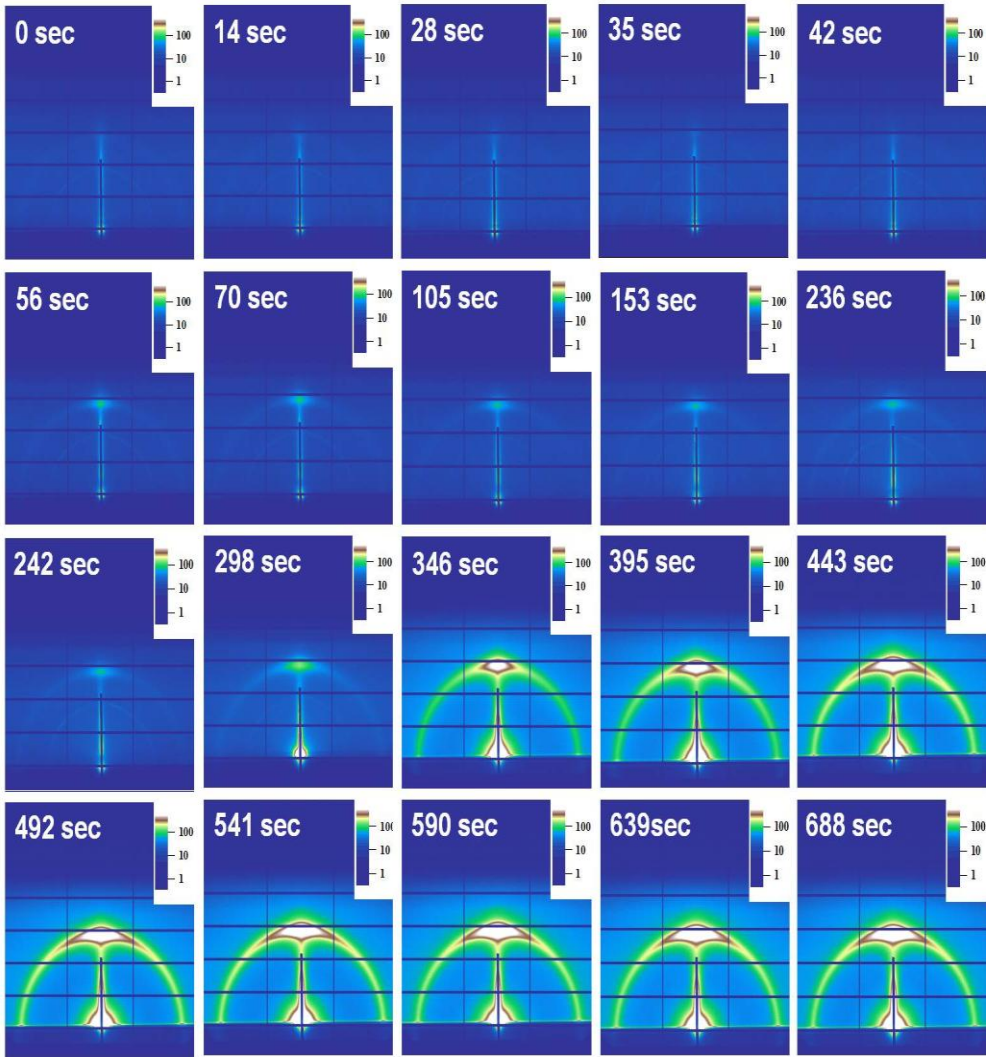

Figure 3.4 Time-resolved GISAXS and GIWAXS image for P3HT/PCBM thin film recorded during solution-casting process

The second step is the initiation of the phase separation and P3HT crystals with various directions and rapid evolution of phase separation and P3HT crystals growth to both directions. In this stage, one interesting point is that the phase separation and P3HT crystals growth according to the both directions is kinetically different meaning that the phase separation and P3TH crystals oriented to the face on direction reach stable state at 492 sec, while P3HT crystals aligned to the edge on direction keep developing. The third step is the direction of the P3HT crystals stop varying and phase separation and P3HT crystals oriented to both directions enter the stable state. As described earlier, the morphology evolution is influenced by the relative solubility difference and the substrate effect. In the same manner, three step morphology evolution of P3HT/PCBM thin film can be demonstrated by making a correlation of each step with those effects. To explain the correlation between morphology evolution in P3HT/PCBM thin film and solubility and substrate effects in detail, the change in invariant, Q of the X-ray scattering as a function of time after casting was plotted (Fig. 3.5). The invariant, Q was obtained by calculating the area under the Lorentz-corrected GISAXS and GIWAXS peaks and it indirectly quantifies the degree of the phase transformation.

$$Q = \int_0^\infty I(q) q^2 dq \tag{3-1}$$

As mentioned above, the first step is the (100) planes in P3HT crystals were seen only at edge-on direction at 56 sec while none of the phase separation and P3HT crystals to the face on direction was observed. The series of invariant Q values shows same trend such that Q value for (100) planes in P3HT crystals to edge on direction slightly increased while Q value for the phase separation and P3HT crystals oriented to face on direction stayed at the initial point. This preferential crystal growth can be explained by the formation of the few P3HT mono layers near the substrate due to the interaction between the P3HT chain and the substrate. From the previous studies, it has been shown that vertical phase separation and P3HT crystal edge on

direction formed during the spin casting process due to the generation of the preferantial interaction between one of the solute materials and the substrate and the creation of repulsive interaction between π electrons in P3HT backbone and the substrate [52,55]. Therefore, in the first stage,P3HT monolayer to the edge on direction forms at the substrate mainly directed by the interaction between solutes components and the substrate, and from the comparison of experimental data and previous studies, phase separation process along the vertical direction is expected as well.

After this slight change, any phase transition was not observed until 298 sec since the significant amount of the solvent still exist and are homogeneously mixed with solutes components. After 298 sec, however, Q values for the phase separation and the P3HT crystals both edge on and face on directions rapidly increased. This is the second step of the morphology evolution in P3HT/PCBM thin film. In this stage, the phase separation process can proceed mainly due to the relative solubility difference to the solvent. Due to PCBM's higher solubility than the P3HT, P3HT is ejected from the homogeneous solution during the solvent evaporation and this ejected P3HT phase enter solidification process faster than the PCBM rich phase - the solubility of the PCBM in chlorobenzene is 42.1 mg/ml and the P3HT is the 14.7 mg/ml [56]. Under the homogeneous mixture state, the crystallization of P3HT is very minimal because of the hindrance of the PCBM. Once the phase separation occurs and the PCBM-rich phase precipitates due to the solubility difference, P3HT crystallization can follow. After 492 sec, the phase separation and the P3HT crystals to face-on direction entered the saturation stage while the P3HT crystals to the edge-on direction kept growing until 590 sec. This result can tells us that the phase separation induced by relative solubility difference is kinetically faster than the P3HT crystallization process. This kinetic result is well matched with phase separation mechanism since phase separation process is mainly done by ejection of P3HT chain from the

homogeneous mixture. These trend can be also seen in Figs. 3.5(b) and 3.5(c) those describe the azimuthal angle-dependent X-ray scattering intensity as a function of time for the edge-on P3HT crystals and the phase separation in the layer respectively.

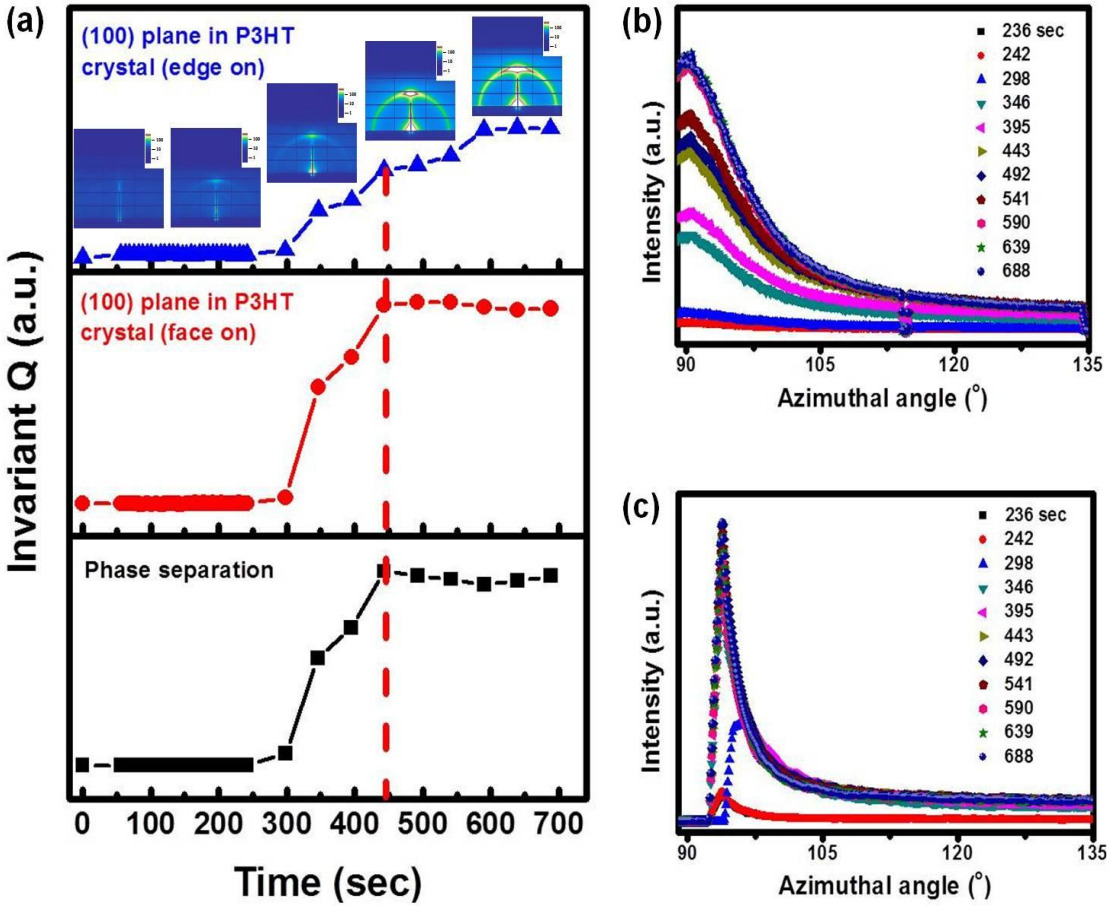

Figure 3.5 The invariant Q value change (a) for phase separation and (100) planes in P3HT crystals to edge and face on direction is displayed as a function of time. Corresponding azimuthal angle distribution for P3HT crystals (b) and phase separation (c). is presented as a function of time.

While the azimuthal angle forP3HT crystals varied from the edge on to the face on direction and the intensity increased until 590 sec, the azimuthal angle for phase separation was quickly reached saturated point at 492 sec. This result can further support the kinetic point of view in second stage such that the P3HT chains crystallized after the P3HT ejection from the homogeneous solution. In third step, the phase separation and P3HT crystal growth reach to the thermodynamically stable stage.

Based on the result of the X-ray scattering, it can conclude that the phase separation along the vertical direction occurs and few P3HT monolayer forms by the substrate effect. When the solvent concentration evaporates further, the phase separation process by the relative solubility difference occurs and P3HT crystallizes right after ejection from the homogeneous mixture.

3.4 Summary

In conclusion, we demonstrated that morphology evolution induced by the phase separation and crystallization process of the P3HT/PCBM thin film by using GISAXS/GIWAXS technique. The spin and solution casting sample was compared to explain the detail progression of the morphology formation. During the film formation under slow solvent evaporation condition, the progression of morphology formation passed three steps to reach stable state. Firstly, the vertical phase separation and formation of few P3HT monolayers oriented to the edge on direction appeared due to the substrate effects. As the solvent evaporates further, the formation of phase separated domains and P3HT crystallization process oriented difference direction was accelerated because of the relative solubility difference in the chlorobenzene. Finally, P3HT crystals oriented to the face on direction and formation of the phase separated domains reached saturation point while P3HT crystals oriented to the edge on direction kept growing. From this result, it can conclude that the PCBM domains are firstly built

by the ejection of P3HT from the homogeneous mixture and P3HT crystal phase are formed after the ejected P3HT chains crystallizes. Based on this morphology study, the right choice of the substrate and solvent can be a key to control the morphology in P3HT/PCBM thin film.

CHAPTER 4

THE STUDY OF PHASE SEPARATION MECHANISM IN P3HT/PCBM BLEND USING TIME-RESOLVED SMALL AND WIDE ANGLE X-RAY SCATTERING

4.1 Introduction

Bulk heterojunction (BHJ) between electron donating- and electron accepting-molecules has been broadly chosen as the most optimized junction structure for organic photovoltaic (OPV) devices because the wide distribution of the junction interfaces in BHJ allows efficient harvesting of the photo-excited excitons with the short diffusion length (10~20 nm) in the molecules [57,58]. BHJ-OPV devices, however, often suffer from low short-circuit current and fill factor due to the difficulty in optimizing the morphology including seemingly randomly distributed junction interfaces. The morphology ultimately optimized for the best efficiency of the device should simultaneously provide large interfacial area and efficient carrier pathway for free charges.

Various approaches have been introduced to build the optimized morphology and they include thermal annealing, solvent annealing, and their variations under a wide range of process variables [59]. As an example, thermal annealing of poly(3-hexylthiophene/[6,6]-phenyl-C61 butyric acid methylester (P3HT/PCBM) BHJ in one of the early studies remarkably improved its power conversion efficiency (PCE) from 0.82 % to almost 3 % and the improvement was primarily ascribed to its morphological change upon annealing - from random mixture to nano-scale phase separation between P3HT- and PCBM-rich domains [60].

Since then, extensive morphology studies have followed exploring the mechanism of the phase separation in BHJs. The phase separation was initially interpreted as a quasi-

eutectic reaction between pure P3HT and PCBM phases. The crystallization of P3HT made understanding of the phase separation process difficult and a series of studies discussed the competition between P3HT crystallization and PCBM diffusion as important parts of the phase separation [61-64]. Chen *et al*. [61] claimed that binodal decomposition between P3HT and PCBM phases was the main mechanism of the phase separation. They supported their conclusion by showing that the formation of the PCBM phase was faster than the crystallization of P3HT and also based on the presence of an activation energy associated with the formation of the PCBM phase - spinodal decomposition is not a thermally activated process.

Unlike Chen *et al*, Wu *et al.* [63] concluded that the phase separation was driven by fast P3HT crystallization and the PCBM phase formed at the P3HT crystal growth front. An in-situ ellipsometry study during the annealing of the P3HT/PCBM BHJ showed that onset of the change in oscillator strength altered by P3HT crystallization was faster than PCBM and proposed the crystallization of P3HT kinetically proceeds the formation of the PCBM phase.

Although it has been shown that the crystallization of P3HT was necessary to optimize PCE of the P3HT/PCBM devices, the amount of the P3HT crystalline phase in the BHJ has not been well quantified. It is worth noting that P3HT crystallinity of about 12% has been reported based on the analysis using transmission electron microscopy and it is possible that the crystallization of P3HT may not be a major part of the phase separation. Morphology of the solution-cast BHJ thin-film is further complicated by the evaporation of solvent and the effect of substrate surface. Friend group in UK emphasized some of these factors and provided a comprehensive picture of the overall phase transformation during the annealing process based on the experimentally obtained depth profiles of the BHJs from ultraviolet and X-ray photoemission spectroscopy [62]. They excluded any major role of the P3HT crystallization in the phase separation by indicating that it would lead to much smaller structures than the 80 nm-

long, vertical, compositional, surface-induced spinodal wave observed from the BHJ. They continued to explain that the wave connected to a continuous binary morphology within the film and the increase of the interfacial area due to the phase separation finally triggered the crystallization of P3HT as a secondary process in the overall process.

In this study, we explored a mechanism of thermally induced phase separation in the mixture of poly(3-alkythiophene) (P3AT) and PCBM by using in-situ small-angle and wide-angle X-ray scattering (SAXS and WAXS) techniques. The diffusion rate of PCBM in the mixture was expected to vary with the length of alkyl group in the polythiophene and the BHJs made with a series of P3AT including poly(3-butylthophene) (P3BT), P3HT, and poly(3-octylthophene) (P3OT) were applied to observe how P3AT crystallization and PCBM aggregation behave under the different PCBM diffusion rate condition on a real-time basis. By comparing P3AT crystallization behavior in P3AT homopolymer and P3AT/PCBM blend, kinetically determined process for phase separation will be examined. Moreover, thermodynamic mechanism for phase separation will be discussed based on the kinetic information of phase separation and P3AT crystallization.

4.2 Experiments

4.2.1 Materials

Regioregular poly(3-hexylthiophene) (P3HT) and [6,6]-phenyl C_{61}-butyric acid methyl ester (PCBM) were purchased from Sigma Aldrich and regioregular poly(3-butylthiophene) (P3BT) and poly(3-octylthiophene) (P3OT) were purchased from Rieke Metals. The reported regioregularity is 80 ~ 90 % for P3BT and 91 ~ 94 % for P3HT and P3OT, and the molecular weight is Mw 50 ~ 70 K for P3BT and P3HT, and Mw 70 – 90 k for P3OT.

4.2.2 SAXS/WAXS

Bulk samples of P3AT/PCBM BHJs were fabricated for SAXS and WAXS experiment. The mixture of P3AT and PCBM at 1:1 ratio was dissolved into chlorobenzene and left under a fume hood until chlorobenzene was completely evaporated. 20 mg of the dried mixture was taken and fabricated into a disc-shape bulk sample for each BHJ and each sample was melt-quenched in liquid nitrogen right prior to the scattering measurement. The X-ray beam line at the Center for Advanced Microstructures & Device (CAMD) in Louisiana State University was used for the scattering experiments and the scattering vector was calibrilated by using silver behenate. The in-situ experiment was conducted at three different isothermal annealing temperatures (110 ^{o}C, 140 ^{o}C, and 170 ^{o}C) by using a hot stage inside a sample chamber. Two different sample-to-detector distances (200 cm and 50 cm) were employed in order to cover a wide range of scattering vector.

4.2 Result and Discussion

Fig. 4.1 displays the Lorentz-corrected SAXS and WAXS data collected from P3HT/PCBM and P3OT/PCBM BHJs during the isothermal annealing at 140 °C together with their time-resolved invariant, Q, which was obtained by integrating the collected data according to Eq. 3.1. As shown in Figs 4.1a and 4.1b, there are mainly two scattering signatures – one at the scattering vector lower than 0.05 Å^{-1} and the other at the vector higher than 0.3 Å^{-1}. These two scattering peaks can be ascribed to the phase separation between P3AT-rich and PCBM-rich domains and the crystalline phase of P3AT respectively [65,66] .

As shown in the Fig. 4.1-(a), two small humps were started to emerge at the 0.038 Å^{-1} and 0.371 Å^{-1} after 1 min annealing. Both peaks were kept growing and moved toward the lower scattering vector side during annealing process. When it reaches 15 min, intensity variation at both sides stopped and the peak positions did not move further and stayed at 0.026 Å^{-1} and

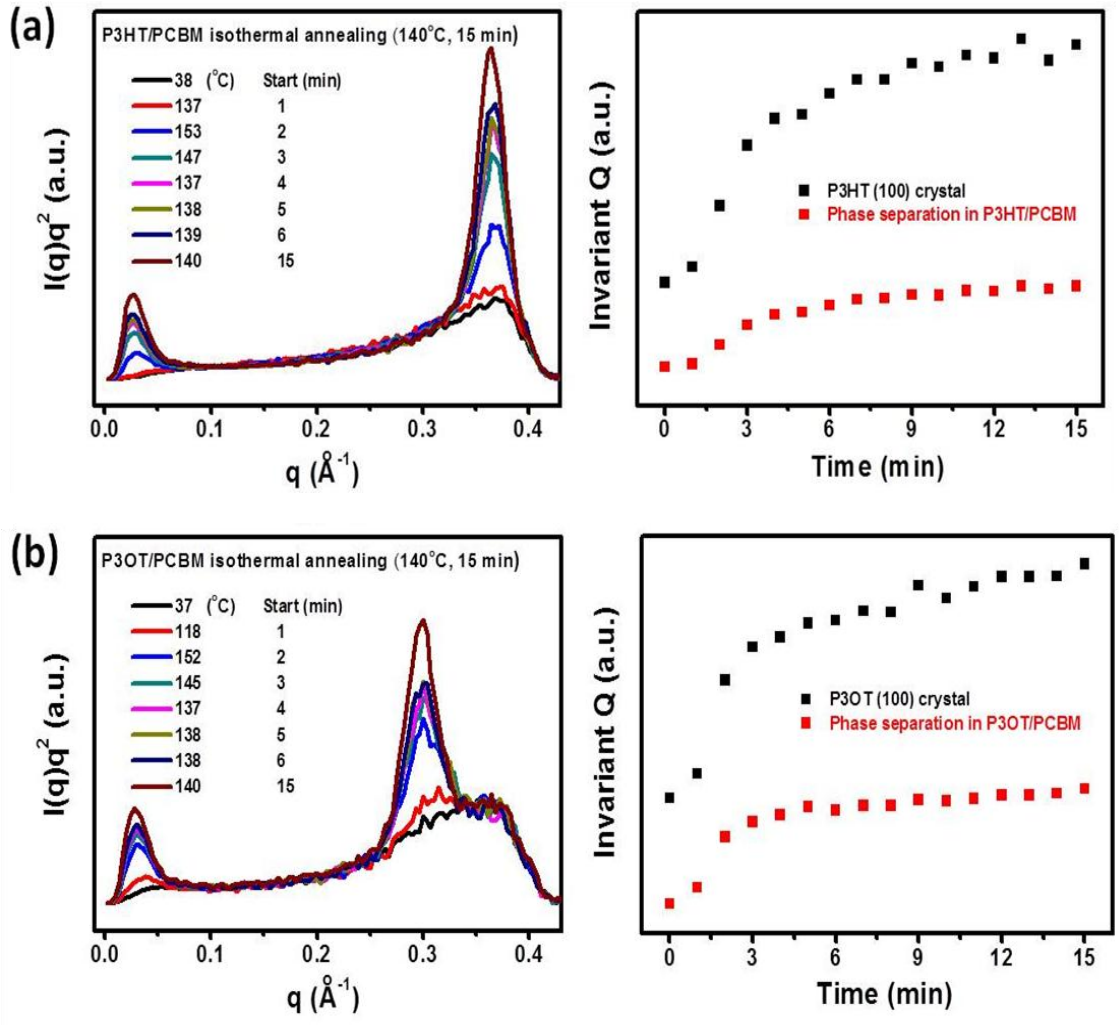

Figure 4.1 In situ X-ray scattering annealed at 140 °C for 15 min (left side) and invariant Q changes as a function of time (right side): (a) P3HT/PCBM and (b) P3OT/PCBM.

0.364 $Å^{-1}$. The calculated long periodicity in the phase separation and the d-spacing of the P3HT crystallites after 15 min annealing were around 23 nm and 2.0 nm respectively which is consistent with previously reported data from P3HT/PCBM BHJs [65,66]. Unlike P3HT/PCBM and P3OT/PCBM BHJs those showed the two signatures of phase separation and

crystallization, P3BT/PCBM did not show any distinctive peak within the entire range of the scattering vector (numbers) of the experiments. The reason for this can be scarce formation of P3BT crystalline phases did not make enough electron density difference between P3BT and PCBM to be detected.

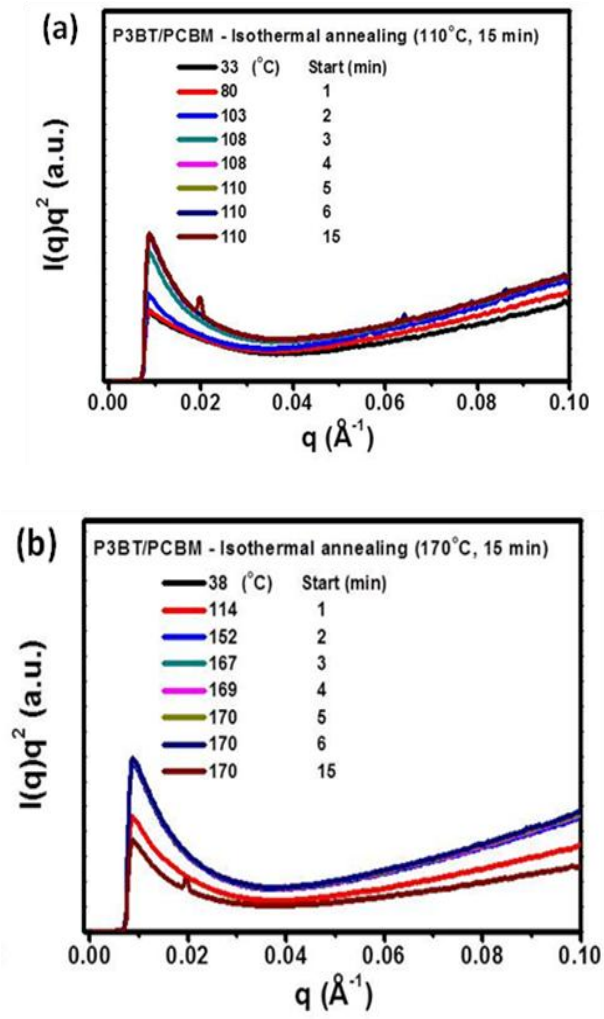

Figure 4.2 In situ X-ray scattering of P3BT/PVBM BHJs annealed at 110 °C for 15 min (a) and 170 °C for 15 min (b)

This time-resolved in-situ SAXS and WAXS result can provide valuable information to understand phase separation mechanism in this complicated binary polymer mixture. Since the invariant Q values stands for the degree of phase separation and P3HT crystallization, AJM equation can be applied to calculate the rate constants for both phase separation and P3HT crystallization. From the direct comparison of the rate constants, it is possible to resolve kinetically determined process for phase separation either PCBM diffusion or P3AT crystallization.

Fig. 4.3 displays P3AT crystallization for both P3AT homopolymers and P3AT/PCBM BHJs progressively changed during the isothermal annealing process. The degree of phase transformation, α(t), was determined by fitting normalized Q vs. time curve using AJM equation,[67-69]

$$\alpha(t) = 1 - \exp(-kt^n) \tag{4-2}$$

where t is the duration of the isothermal annealing, k is a rate constant, and n is AJM constant. The rate constants extracted for P3AT crystallization were compiled in Table 1. Comparison of the rate constants for the P3AT crystallization in both homopolymer and BHJ shows that its crystallization rate depends on the presence of PCBM. For example, P3HT crystallization reached its saturation within 5 min of the annealing process while P3OT took more than 30 min. In P3AT/PCBM blend, however, P3OT crystallized faster than P3HT unlike the crystallization of the homopolymers without PCBM. This reversal trend of crystal growth can provide an answer for kinetically determined process for phase separation in P3AT/PCBM blend. Since the diffusion of PCBM during the annealing process hinders both P3AT's nucleation and polymer chain diffusion to the growth front, P3AT crystal growth rate in P3AT/PCBM is diminished. This change can be explained by that PCBM diffusion to form PCBM rich phase preceded the P3AT crystallization - If P3AT crystallization occurred faster than the phase separation in the

BHJs, the P3AT crystallization kinetics would have followed the same trend with P3AT homopolymers.

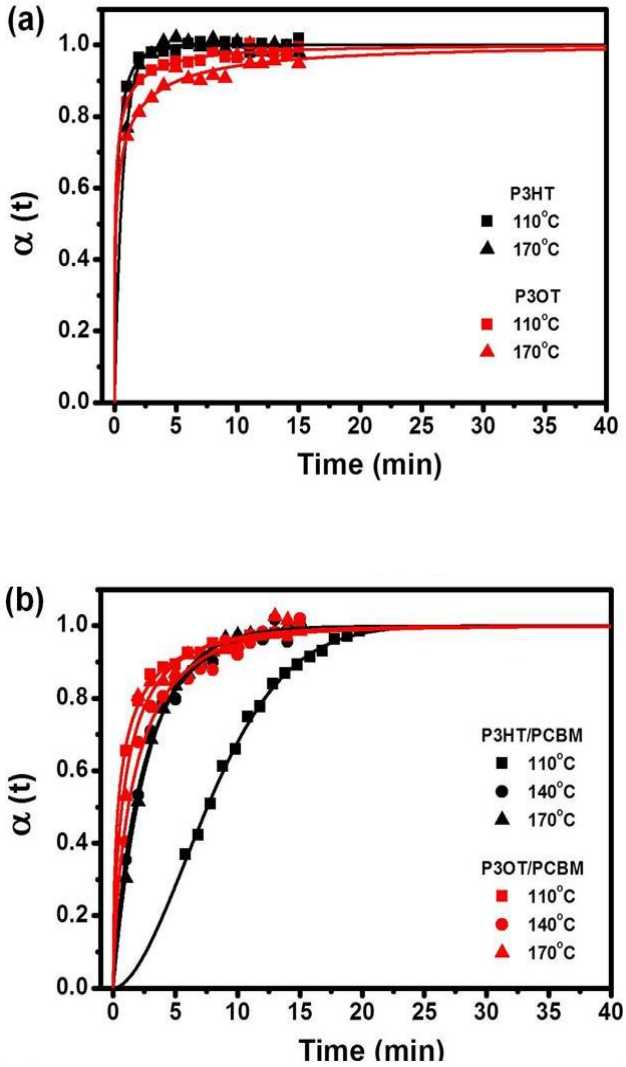

Figure 4.3 Plot of extent of P3AT crystallization (a) and P3AT crystallization (b) in P3AT/PCBM blend respectively displayed as a function of time at different annealing temperature: The black color stands for P3HT or P3HT/PCBM blend and red color stands for P3OT or P3OT/PCBM blend. The solid square, circle, and triangle means 110 °C, 140 °C, 170 °C thermal annealing condition respectively.

Table 1. Rate constants of crystallization in P3HT and P3OT homopolymers and their BHJs with PCBM.

Temperature [°C]	P3HT	P3OT	P3HT/PCBM	P3OT/PCBM
110	2.197	1.837	0.019	1.101
140			0.447	0.612
170	1.460	1.363	0.377	0.868

To study phase separation mechanism of P3HT/PCBM blend, the reason for peak evolution at small angle side and image of P3HT/PCBM blend using Force Modulation Microscopy (FMM) were analyzed. As shown in Fig. 4.1, the two scattering peaks were emerged from the small angle and wide angle side which are assigned to phase separation and P3AT crystallization. In SAXS/WAXS technique, the reason for peak evolution at small angle side was due to presence of alternated structure between P3HT rich- and PCBM rich phase with long range density fluctuations. FFM image (Fig. 4.3) of P3HT/PCBM blend after thermal annealing (140 °C for 15 min) further confirms evolution of alternated structure. Since the PCBM is stiffer than the P3HT [70], the dark area stands for PCBM phase while the bright area stands for P3HT phase. One of the characteristic for spinodal decomposition is formation of alternated structure with long range density fluctuation during phase separation while the nucleation and growth mechanism shows evolution of phase separated structure in a random manner [71]. Based on results from peak evolution at small angle side and FFM image, it can be inferred that spinodal decomposition is the main mechanism of phase separation in P3AT/PCBM blend during thermal annealing process.

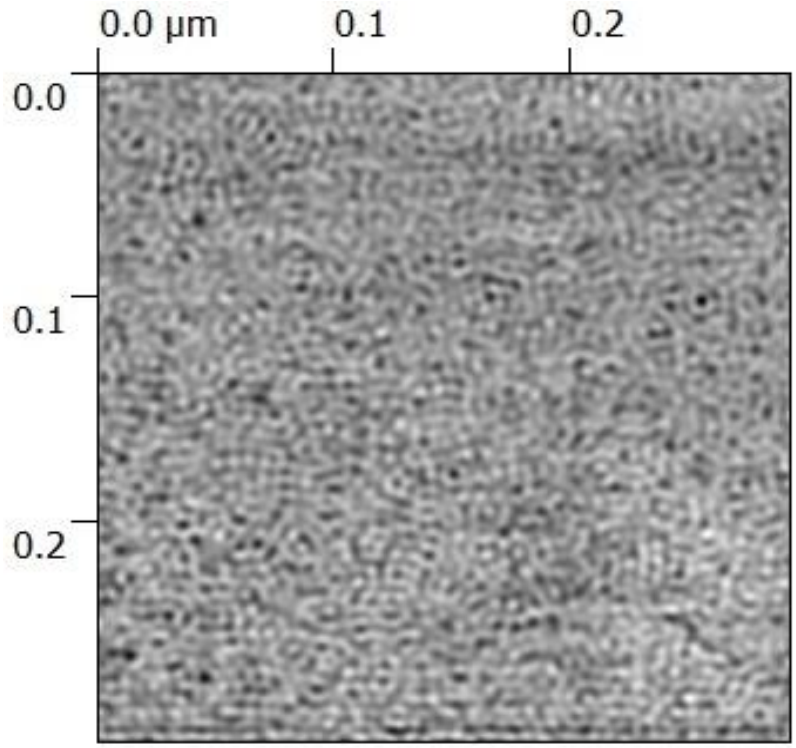

4.3 FMM image of P3HT/PCBM blend after thermal annealing at 140 °C for 15 min.

4.4 Summary

In summary, we measured phase separation and crystallization of P3AT/PCBM simultaneously using SAXS and WAXS technique. Based on results of rate constants extaracted from AJM eqaution, kinetically-determined process for phase separation can be resolved. From the observation of variation of P3AT crystallization rate with and without the PCBM molecules, it can demonstrate that the PCBM diffusion is kinetically determined process during the phase separation of P3AT/PCBM blend.

Moreover, analysis of peak evolution at small angle side combined with FFM image, it can conclude that the mechanism for phase separation in P3AT/PCBM blend is spindal decomposition. Hence, the morphology formation in P3AT/PCBM blend during the thermal

annealing process passes two steps. The first step is phase separation mainly driven by PCBM diffusion, producing PCBM rich and P3AT rich phase. The mechanism of this phase separation is spinodal decomposition. The second step is P3AT crystallization process.

CHAPTER 5

THE STUDY OF MORPHOLOGY EFFECTS ON EFFICIENCY OF P3AT/PCBM SOLAR CELL

5.1 Introduction

Although it was well understood that the phase separated morphology was directly related with the cell performance, the solar cell efficiency is often optimized by a trial and error method due to a lack of fundamental studies. For example, P3HT/PCBM solar cell fabricated by post thermal treatment (140 ^{o}C for 15 min) after the thin film deposition showed the best cell performance, compared with other experimental condition due to formation of large interfacial area as well as efficiency charge carrier pathway [72]. This morphology condition can be achieved by nano-scale phase separation and P3HT crystallization process during thermal annealing process. However, it has been still unknown that how this morphology condition affects on the solar cell efficiency in detail manner. For example, it is still far from the clear what morphology condition are making best cell performance and what factors influence more dominantly on the device performance either phase separation or crystallization. Hence, the detail explanation for the relationship between morphology condition and device performance is highly necessary.

In this study, the invariant (Q) and long periodicity value extracted from SAXS/WAXS technique were applied and compared with device electronic parameters in order to examine morphology effects on efficiency of P3AT/PCBM solar cell. Here, both Q and long periodicity value indicate the degree of crystalline phases and phase separation length respectively, which

determines free charge carrier conduction and excitons dissociation rate. P3HT/PCBM and P3OT/PCBM solar cell were prepared with various annealing temperature to study morphology effects on solar cell performance.

5.2 Experiments

5.2.1 Solar Cell fabrication

The solar cell was prepared by the blend solution (P3AT : PCBM = 1:1 by weight) and chlorobenzene was used as solvent. Indium tin oxide (ITO) coated glass was cleaned by soap water, toluene, acetone, and isopropanol respectively under the ultrasonic bath for 20 min. Poly(3,4-ethylenedioxythiophene) poly(styrenesulfonate) (PEDOT:PSS) and P3HT PCBM blend solution was spin coated 5000 rpm and 1500 rpm respectively. Calcium and Aluminum was deposited by thermal evaporator.

5.2.2 Current-Voltage Measurement

The current density and voltage (I-V) measurement was conducted under air mass (AM)0 condition. I-V of organic solar cell was measured by home-made solar simulator using a Keithley 2420 3A source meter controlled by computer program written by NASA Glenn Research Center. Projector lamp is calibrated for (AM)0 using the crystalline silicon solar cell calibrated by NASA Glenn Research Center.

5.3 Result and Discussion

In order to understand the morphology effects on device performance, invariant (Q) and long periodicity changes according to the annealing temperature and time were displayed in Fig. 5. Here, Q and long periodicity can stand for the degree of P3AT crystallization and phase separation in P3AT/PCBM blend, which are factors determining charge conduction and excitons dissociation respectively. From the result of Fig. 5, P3HT/PCBM annealed at 140 °C showed

the highest degree of P3AT crystallization, meaning that the most efficient pathway was built, compared with other experimental condition.

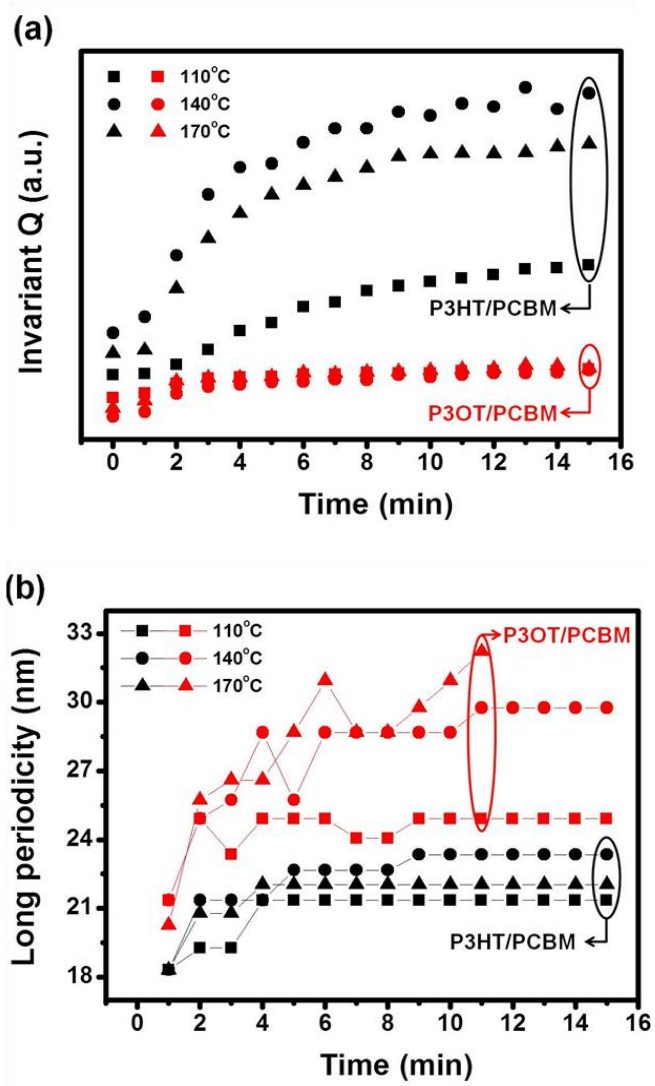

Figure 5.1 Invariant Q (top) and long periodicity (bottom) value change as a function of time: solid square (110 ^{o}C for 15 min annealing), solid circle (140 ^{o}C for 15 min annealing), and solid triangle (170 ^{o}C for 15 min annealing).

As discussed in chapter 4, the diffusion of PCBM highly depends on the side alkyl chain length. Therefore, the PCBM-rich domains appeared much rapidly for P3OT/PCBM and the longer periodicity of P3OT/PCBM is also expected from larger PCBM domains. Because the long periodicity in P3OT/PCBM BHJ is longer than that of P3HT/PCBM and the typical diffusion length of an exciton is between 10 nm and 20 nm, excitons generated in P3OT/PCBM BHJ (the blend with longer side alkyl chain) will suffer more recombination than P3HT/PCBM during their diffusion to reach the interface between P3OT-phase and the PCBM-phase. The previous study often indicated that P3HT/PCBM BHJs show superior performance over P3OT/PCBM BHJs [73] and the Q and long periodicity could explain the reason.

The Fig. 6 and table 2 showed I-V characteristic of the OPV device with different experimental condition. The result of the efficiency of P3AT/PCBM solar cell indicated that P3HT/PCBM mixture showed better cell performance than P3OT/PCBM. This can be successfully explained by invariant Q value and long periodicity range change which was discussed in Fig. 5. The sample annealed at 140 ^{o}C showed highest amount of crystalline phase among all the other samples and calculated long periodicity between P3HT and PCBM rich domain was 23.3 nm which satisfies the typical excitons diffusion length (~5 to 20 nm) [74] while P3OT/PCBM had the smaller crystalline phase and the larger longer periodicity.

These resulted data can tell us that the charges separation and their conduction was performed most efficiently under 140 ^{o}C annealing condition with P3HT/PCBM sample. The cell result follow the expectation extracted from the invariant Q and long periodicity data. From the table 2, the V_{oc} and J_{sc} was dropped significantly from 0.59 V and 6.62 mA cm^{-2} to 0.34 V and 1.55 mA cm^{-2} between P3HT/PCBM and P3OT/PCBM annealed at 140 ^{o}C. Since V_{oc} and J_{sc} are highly affected by charges separation and theirs collection, the reason for huge drop is that

longer periodicity and scarce of crystalline phase hinder the charge separation and charge carries conduction to the both electrodes.

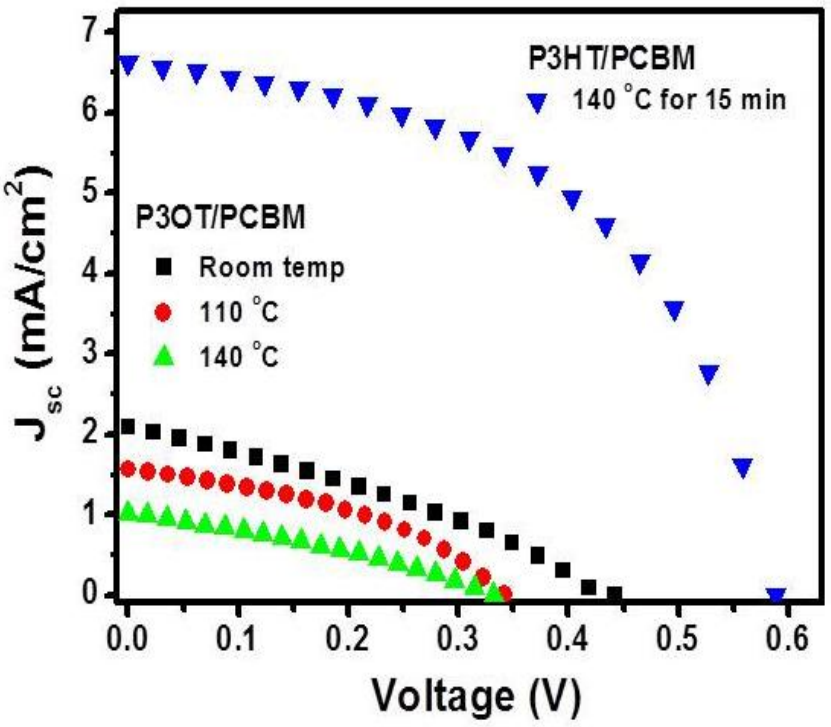

Figure 5.2 Current - voltage characteristic curve for P3HT/PCBM and P3OT/PCBM (AM-0 condition).

Table 2. Device electronic parameters at different annealing temperature.

Sample	Annealing Temp. [^{o}C]	V_{oc} [V]	J_{sc} [mA cm^{-2}]	FF	Efficiency [%]	Condition
P3HT/PCBM	140	0.59	6.62	0.51	1.47	AM 1.0
P3OT/PCBM	Non-annealled	0.44	2.08	0.31	0.21	AM 1.0
P3OT/PCBM	110	0.34	1.55	0.40	0.16	AM 1.0
P3OT/PCBM	140	0.33	1.01	0.32	0.08	AM 1.0

Furthermore, P3OT/PCBM provides more interesting feature regarding the importance of charge separation or carriers conduction. After 15 min annealing regardless of the annealing temperature, invariant Q values had almost same value while the long periodicity values were varied from 32.2 nm to 24.9 nm at 170 ^{o}C and 110 ^{o}C respectively.

From table 2, J_{sc} and V_{oc} also dropped as long periodicity value increased. This is highly possible that generated excitions inside P3OT were mostly recombined on the way to PCBM interface before they were separated. Moreover, this PCE drop can tell us that degree of phase separation is more crucial factor for the PCE rather than amount of crystalline phase inside of BHJs. This also can be the answer for the question such that why BHJs blended with amorphous low band gap polymer still shows superior device performance without crystalline phase. [75-78]

5.4 Summary

Based on invariant Q and long periodicity value calculated from SAXS/WAXS technique, morphology effects on the P3AT/PCBM solar cell were investigated. From the fact that P3HT/PCBM blend annealed at 140 °C showed best solar cell performance, compared with other experimental condition, excitons dissociation and charge conduction to both electrodes was expected to perform most efficiently. Since it has moderate long periodicity and the highest amount of crystalline phase, it is found out that both phase separation length and amount of P3HT crystalline phase make contribution to enhance the excitons dissociation rate and hole mobility respectively

Moreover, further study using P3OT/PCBM blend showed that nano-scale phase separation plays key role in terms of device performance than the crystalline phase. This finding was obtained from the facts the efficiency of P3OT/PCBM solar cell dropped as long periodicity value increased while amount of P3OT crystalline phase was same. . This result

can be a reason why recent OPV device fabricated with low band gap polymer shows decent performance without crystalline phase.

CHAPTER 6

CONCULSION AND FUTURE WORK

6.1 Conclusion

The ultimate goal of this study is to investigate the morphology evolution of a polymer-fullerene blend and morphology effects on device performance. The primary focus on this study is to identify a phase separation mechanism (binodal or spinodal decomposition) and its driving force (polymer crystallization or PCBM diffusion) in a polymer-fullerene blend system during film deposition and post thermal treatment. Also, the morphology effects on OPV device performance are studied.

6.1.1 Morphology Evolution in Solution-Casted P3HT/PCBM Thin Film

Our exploration with GISAXS and GIWAXS technique found that the polarity of the substrate, a solubility, and solvent evaporation time determine the P3HT/PCBM morphology. On the basis of the results of the peak evolution with time at small and wide angle during the film deposition under slow solvent evaporation condition, the progression of morphology formation passed three steps to reach stable state. Firstly, the vertical phase separation and few P3HT monolayers oriented to the edge on direction are formed due to the substrate effects. Secondly, the solubility difference accelerates formation of phase separated domains and P3HT crystallization process oriented to various direction. Finally, P3HT crystals oriented to the face on direction and formation of the phase separated domains reached saturation point. Based on

this morphology study, the right choice of the substrate and solvent can be a key to control the morphology in P3HT/PCBM thin film.

6.1.2 Phase Separation Mechanism in P3AT/PCBM Blend

Spinodal decomposition was found to be mechanism for the phase separation of P3AT/PCBM blend. During the post thermal treatment, PCBM and P3AT-rich phase was formed first by spinodal decomposition, kinetically driven by PCBM diffusion process. Thereafter, P3AT crystallization occurs from the place where PCBM diffused out. This finding was obtained from the facts that rate constants of PCBM diffusion is faster than P3AT crystallization process and alternating structure with long range order was evolved during the thermal annealing.

6.1.3 Morphology Effects on Performance of P3AT/PCBM Solar Cell

From the direct comparison of long periodicity and invariant Q to solar cell efficiency, the importance of the phase separation and P3AT crystallization on the solar cell efficiency was investigated. It is found out that both phase separation length and degree of P3AT crystallization make contribution to increase the solar cell efficiency by enhancing exciton dissociation rate and hole mobility. Moreover, further study using P3OT/PCBM solar cell showed that phase separation length plays a vital role to determine performance of OPV device more than P3AT crystalline phase. This result can be a reason why recent OPV device fabricated with low band gap polymer shows decent performance without crystalline phase.

6.2 Future Work

In P3AT/PCBM, PCE is enhanced when post treatments such as thermal or solvent-vapor annealing are applied. The origin of this improvement is formation of phase separated area as well as P3HT crystals in face-on direction during the post treatments, enhancing excitons dissociation rate and hole mobility respectively [79].

6.2.1 Control of Hole Mobility

It was previously shown that the P3HT/PCBM solar cell, containing more crystalline phase oriented to face-on direction showed fast hole mobility than the one with less amount of face-on direction crystalline phase since the holes can travel fast to the anode through the π-π stacking perpendicular to the substrate and the face-on P3HT crystals also lower the contact resistance between active layer and electrode. From the scattering result, however, there still exist significant amounts of the P3HT crystals oriented to the edge on direction compared with one which oriented to the face on direction even though the slow solvent evaporation process is applied. Moreover, during the vertical phase separation directed by the substrate, more PCBM contents are observed near the substrate side when polar substrate used and this higher concentration near substrate can disturb the holes collection to the anode side. In order to enhance the PCE further, it is recommended to fabricate P3HT/PCBM thin film which has higher amounts of the P3HT crystals oriented to the face on direction and make higher PCBM concentration near the surface of the film. These necessary condition can be achieved by changing the polarity of substrate and manipulate the surface energy of the solute materials. The previous studies have shown that direction of poly(3,3'''-didodecylquaterthiophene), (PQT-12) crystals is controlled by changing the surface chemistry of the substrate. The PQT-12 crystals grown on substrate modified by octyltrichlorosilane showed highly oriented to the edge on direction which is favored for the organic thin film transistor and the mobility enhancement around 450 times faster than the one grown on the non modified substrate [80].

6.2.2 Control of Vertical Phase Separation

The vertical phase separation occurs because of the difference of surface energy for solutes materials. In P3AT/PCBM thin film, due to the higher surface energy of PCBM than P3AT, P3AT tends to stay at the surface side of the film while the PCBM is located on the

substrate side during the morphology evolution. Sine PCBM and P3HT phase conducts the electron and hole to cathode and anode respectively, vertical phase separation (P3AT top and PCBM bottom) is not favored direction in terms of efficiency of organic solar cell. In order to fabricate the film such that the location of PCBM is top and P3HT bottom which is favored for organic solar cell, high pressurized CO_2 gas is introduced to the P3HT/PCBM thin film since the CO_2 gas makes PCBM plasticize only leading to lower the surface energy, and this surface energy change adjust the location of the PCBM and the P3HT reversely [81]. To author's knowledge, it is still challengeable to control both directions of crystal and vertical phase separation simultaneously.

REFERENCES

[1] R. Gaudiana and C. Brabec, Nature Photonics **5,** 287(2008).

[2] R. Søndergaard, M. Helgesen, M. Jørgensen, and F. C. Krebs, Adv. Energy Mater. **1**, 68 (2011).

[3] S. H. Park, A. Roy, S. Beaupré, S. Cho, N. Coates, J. S. Moon, D. Moses, M. Leclerc, K. Lee, and A. J. Heeger, Nature Photonics **5**, 297 (2009).

[4] Y. Liang, Z. Xu, J. Xia, S.-T. Tsai, Y. Wu, G. Li, C. Ray, and L. Yu. Adv. Mater. **22**, E135 (2010).

[5] J. Hou, H.-Y. Chen, S. Zhang, G. Li, and Y. Yang. J. Am. Chem. Soc. **130**, 16144 (2008).

[6] H.-Y. Chen, J. Hou, S. Zhang, Y. Liang, G. Yang, Y. Yang, L. Yu, Y. Wu, and G. Li, Nature Photonics **3**, 649 (2009).

[7] G. Li, C.-W. Chu, V. Shrotriya, J. Huang, and Y. Yang, Appl. Phys. Lett. **88**, 253503 (2006).

[8] K.-S. Shin, K.-H. Lee, H. H. Lee, D. Choi, and S.-W. Kim, J. Phys. Chem. C, **114**, 15782 (2010).

[9] W. Ma, C. Yang, X. Gong, K. Lee, A. J. Heeger, Adv. Funct. Mater. **15**, 1617 (2005).

[10] J. M. Nunzi, Comptes Rendus Physique **3**, 523 (2002).

[11] R. J. Hoffmann, R. Janiak, C. Kollmar, Macromolecules **24**, 3725-3746 (1991).

[12] H. Sirringhaus, P. J. Brown, R. H. Friend, J. Nielsen, K. Bechgaard, B. M. W. Langeveld-Voss, A. J. H. Spiering, R. A. J. Janssen, E. W. Meijer, P. Herwig, D. M. de Leeuw, Nature **401**, 685-688 (1999).

[13] B. C. Thompson, and J. M. J. Frechet, Angew. Chem. Int. Ed. **47**, 58 (2008).

[14] A. L. Ayzner, C. J. Tassone, S. H. Tolbert, and B. J. Schwartz, J. Phys. Chem. **113**, 20050 (2009).

[15] L. M. Andersson, C. Muller, B. H. Badada, F. Zhang, U. Wurfel, and O. Inganas, J. Appl. Phys. **110**, 024509 (2011).

[16] S. V. Bavel, S. Veenstra, J. Loos, Macromol. Rapid Commun, **31**, 1835 (2010).

[17] N. Dobre, P. Denk, S. Boudiba, M. Scharber, N. S. Sariciftci, D. A. M. Egbe, M. Buda, Dige. Jour. Nano. Bios. **8**, 1475 (2013).

[18] H.-J. Jhuo, P.-N. Yeh, S.-H. Liao, Y.-L. Li, Y.-S. Cheng, S.-A. Chen, Jour. Chin. Chem. Soci. **60**, 2192 (2013).

[19] C. Kastner, B. Muhsin, A. Wild, D. A. M. Egbe, S. Rathgeber, H. Hoppe, J. Polym. Scie. Part B. **51**, 868 (2013).

[20] H. Hoppe, and N. S. Sariciftci, J. Mater. Res. **19**, 1928 (2004).

[21] M. C.-Quiles, T. Ferenczi, T. Agostinelli, P. G. Etchegoin, Y. Kim, T. D. Anthopoulos, P. N. Stavrinou, D. D. C. Bradley, and J. Nelson, *Nature Materials* **7**, 158 (2008).

[22] Y. Vaynzof, D. Kabra, L. Zhao, L. L. chua, U. Steiner, and R. H. Friend, *ACS Nano* **5**, 329 (2011).

[23] W.-R. Wu, U-S. Jeng, C.-J. Su, K.-H. Wei, M.-S. Su, M.-Y Chiu, C.-Y. Chen, W.-B. Su, C.-H. Su, and A.-C. Su, *ACS Nano* **5**, 6233 (2011).

[24] D. Chen, A. Nakahara, D. Wei, D. Nordlund, and T. P. Russell, *Nano Lett.* **11**, 561(2011).

[25] W. Y. Huang, C. C. Lee, S. G, Wang, Y. K Han, and M. Y. Chang, J. Electrochem. Soc. **157**, B1336 (2010).

[26] O. Glatter and O. Kratky, Small Angle X-ray Scattering, p.18 (1982).

[27] A. A. Herzing, L. J. Richter, and I. M. Anderson, J. Phys. Chem. C. **114**, 17501 (2010).

[28] M. Y. Chiu, U. S. Jeng, C. H. Su, K. S. Liang, and K. H. Wei, Adv. Mater. **20**, 2573 (2008).

[29] P.G. Karagiannis, S. Kassavetis, C. Pitsalidis, and S. Logothetidis, Thin Solid Films **519**, 4105 (2011).

[30] http://www.parkafm.com/AFM_guide/spm_modes_8.php?id=1215

[31] M. P. Nikiforov, S. B. Darling , J. Vis Exp. **71**, e50293 (2013).

[32] S. D. Baranovskii, M. Wiemer, A.V. Nenashev, F. Jansson, and F. Gebhard, J. Phys. Chem. Lett. **3**, 1214 (2012).

[33] P.G. Karagiannidis, S. Kassavetis, C. Pitsalidis, and S. Logothetidis, Thin Solid Films **519**, 4105 (2011).

[34] G. Li, R. Zhu, and Y. Yang, Nature Photonics **6**, 153 (2012).

[35] H. Hoppe, and N. S. Sariciftci, J. Mater. Chem. **16**, 45 (2006).

[36] C. J. Brabec, S. Gowrisanker, J. J. M. Halls, D. Laird, S. Jia, S. P. Williams, Adv. Mater. **22**, 3839 (2010).

[37] S. Günes, H. Neugebauer, ad N. S. Sariciftci, Chem. Rev. **107**, 1324 (2007).

[38] F. - C. Chen, C. - J. Ko, J. - L. Wu, and W. - C. Chen, Solar Energy Materials & Solar Cells **94**, 2426 (2010).

[39] X. Fan, G. J. Fang, P. L. Qin, F. Cheng, X. Z. Zhao, Appl. Phys. A **105**, 1003 2011.

[40] Y. - M. Shen, C. - S. Chen, P. – C. Yang, S. - Y. Ma, and C. – F. Lin, Solar Energy Materials & Solar Cells **99**, 263 (2012).

[41] J. H. Park, J. S. Kim, J. H. Lee, W. H. Lee, K. Cho, J. Phys. Chem. C **113**, 17579 (2009).

[42] E. Verploegen, C. E. Miller, K. Schmidt, Z. Bao, and M. F. Toney, Chem. of Mater. **24**, 3923 (2012).

[43] S. Walheim, M. Böltau, J. Mlynek, G. Krausch, and U. Steiner, Macromolecules **30**, 4995 (1997).

[44] S. Nilsson, A. Bernasik, A. Budkowski, and E. Moons, Macromolecules **40**, 8291 (2007).

[45] Y.-M. Chang and L. Wang, J. Phys. Chem. C **112**, 17716 (2008).

[46] S. Miller, G. Ganchini, Y.-Y. Lin, C. Li, C.-W. Chen, W.-F. Su, and M. Chhowalla, J. Mater. Chem. **18**, 306 (2008).

[47] Y. Vaynzof, D. Kabra, L. Zhao, L. L. Chua, U. Steiner, and R. H. Friend, ACS Nano **5**, 329 (2011).

[48] M. C.-Quiles, T. Ferenczi, T. Agostinelli, P. G. Etchegoin, Y. Kim, T. D. Anthopoulos, P. N. Stavrinou, D. D. C. Bradley, and J. Nelson, Nature Materials **7**, 158 (2008).

[49] W.-R. Wu, U-Ser Jeng, C.-J. Su, K. H. Wei, M.-S. Su, M.-Y. Chiu, C.-Y. Chen, W.-B. Su, C.-H. Su, and A. C. Su, ACS NANO, **8**, 6233 (2011).

[50] T. Agostinelli, S. Lilliu, J. G. Labram, M. C.-Quiles, M. Hampton, E. Pries, J. Rawle, O. Bikondoa, D. D. C. Bradley, T. D. Anthopoulos, J. Nelson, and J. E. Macdonald, Adv. Funct. Mater. **21**, 1701 (2011).

[51] M.-Y. Chiu, U.-S. Jeng, M.-S. Su, K.-H. Wei, Macromolecules, **43**, 428 (2010).

[52] K. W. Chou, B. Yan, R. Li, E. Q. Li, K. Zhao, D. H. Anjum, S. Alvarez, R. Gassaway, A. Biocca, S. T. Thoroddsen, A. Hexemer, and A. Amassian, Adv. Mater. **25**, 1923 (2013).

[53] A. J. Parnell, A. J. Cadby, O. O. Mykhaylyk, A. D. F. Dunbar, P. E. Hopkinson, A. M. Donald, and R. A. L. Jones, Macromolecules, **44**, 6503 (2011).

[54] S. Kim, J. K. Lee, M. H.-C. Jin, 38th IEEE Photovoltaic Specialists Conference, 003044 (2012).

[55] D. H. Kim, Y. Jang, Y. D. Park, K. Cho, Langmuir, **21**, 99 (2005).

[56] F. Machui, S. Langner, X. Zhu, S. Abbott, and C. J. Brabec, Solar Energy Materials and Solar Cells **100**, 138 (2012).

[57] R. Gaudiana and C. Brabec, Nature Photonics **5**, 287 (2008).

[58] R. Søndergaard, M. Helgesen, M. Jørgensen, and F. C. Krebs, Adv. Energy Mater. **1**, 68 (2011).

[59] H. Hoppe and N. S. Sariciftci, J. Mater. Chem. **16**, 45 (2008).

[60] W. Ma, C. Yang, X. Gong, K. Lee, and A. J. Heeger, Adv. Funct. Mater. **15**, 1617 (2005).

[61] M. C.-Quiles, T. Ferenczi, T. Agostinelli, P. G. Etchegoin, Y. Kim, T. D. Anthopoulos, P. N. Stavrinou, D. D. C. Bradley, and J. Nelson, Nature Materials **7**, 158 (2008).

[62] Y. Vaynzof, D. Kabra, L. Zhao, L. L. chua, U. Steiner, and R. H. Friend, ACS Nano **5**, 329 (2011).

[63] W.-R. Wu, U-S. Jeng, C.-J. Su, K.-H. Wei, M.-S. Su, M.-Y Chiu, C.-Y. Chen, W.-B. Su, C.-H. Su, and A.-C. Su, ACS Nano **5**, 6233 (2011).

[64] D. Chen, A. Nakahara, D. Wei, D. Nordlund, and T. P. Russell, Nano Lett. **11**, 561 (2011).

[65] A. J. Parnell, A. J. Cadby, O. O. Mykhaylyk, A. D. F. Dunbar, P. E. Hopkinson, A. M. Donald, and R. A. L. Jones, Macromolecules **44**, 6503 (2011).

[66] T. Agostinelli, S. Lilliu, J. G Labram, M. C.-Quiles, M. Hampton, E. Pires, J. Rawle, O. Bikondoa, D. D. C. Bradley, T. D. Anthopoulos, J. Nelson, and J. E. Macdonald, Adv. Funct. Mater. **21**, 1701 (2011).

[67] S hugger, R. Thomann, T. Heinzel, and T. T.-Albrecht, Colloid Polym. Sci. **282**, 932 (2004).

[68] M. Avrami, J. Chem. Phys. **7**, 1103 (1939).

[69] M. Avrami, J. Chem. Phys. **8**, 212 (1940).

[70] P. G. Karagiannidis, S. Kassavetis, C. Pitsalidis, S. Logothetidis, Thin Solid Films **519**, 4105 (2011).

[71] H. Wang, Polymer **47**, 4897 (2006).

[72] Y. Kim, S. A. Choulis, J. Nelson, D. D. C. Bradley, S. Cook, and J. R. Durrant Appl. Phys. Lett. **86**, 063502 (2005).

[73] L. H. Nguyen, H. Hoppe, T. Erb, S. Gunes, G. Gobsch, and N. S. Sariciftci, Adv. Funct. Mater. **17**, 1071 (2007).

[74] T. Kietzke, R. Y. C. Shin, D. A M. Egbe, Z.-K. Chen, and A. Sellinger, Macromolecules **40**, 4424 (2007).

[75] E. Bundgaard, F. C. Krebs, Solar Energy Materials & Solar Cells **91**, 954 (2007).

[76] E. Bundgaard, F. C. Krebs, Solar Energy Materials and Solar cells **91**, 954 (2007).

[77]. D. Mühlbacher, M. Scharber, M. Morana, Z. Zhu, D. Waller, R. Gaudiana, and C. Brabec, Adv. Mater. **18**, 2884 (2006).

[78] J. Peet, J. Y. Kim, N. E. Coates, W. L. Ma, D. Moses, A. J. Heeger, and G. C. Bazan, Nature Materials **6**, 49 (2007).

[79] N. D. Treat, C. G. Shuttle, M. F. Toney, C. J. Hawker and M. L. Chabinyc, J. Mater. Chem.

21, 15224 (2011).

[80] Y. Wu, P. Liu, B. S. Ong, T. Srikumar, and N. Zhao, Appl. Phys. Lett. **86**, 142102 (2005).

[81] R. Kokubu, and Y. Yang, Phys. Chem. Chem. Phys. **14**, 8313 (2012).

BIOGRAPHICAL INFORMATION

Soo Kim, received his Bachelor's degree of Bio-chemical Engineering from Chosun University, from South Korea in 2007. After he finished his bachelor degree, he started his graduate study at University of Texas in Arlington in 2008 to pursue his Ph.D in Materials Science and engineering. He started his BS-Ph.D program joined the Photovoltaics group headed by Dr. Michael Jin in August 2008 and earned Ph.D degree under Dr. Choong-Un Kim supervision. His research interest is phase transformation of an active layer in organic photovoltaic device as well as morphology effects on organic photovoltaic device performance.